




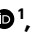






Neurotensin neurons in the extended amygdala control dietary choice and energy homeostasis

Received: 11 September 2021

Accepted: 6 September 2022

Published online: 20 October 2022

 Check for updates

Alessandro Furlan ^{1,5}✉, Alberto Corona ^{1,2,6}, Sara Boyle ^{1,2,6}, Radhashree Sharma¹, Rachel Rubino ¹, Jill Habel¹, Eva Carlotta Gablenz ^{1,3}, Jacqueline Giovanniello ^{1,2}, Semir Beyaz ¹, Tobias Janowitz ^{1,4}, Stephen David Shea ¹ and Bo Li ¹✉

Obesity is a global pandemic that is causally linked to many life-threatening diseases. Apart from some rare genetic conditions, the biological drivers of overeating and reduced activity are unclear. Here, we show that neurotensin-expressing neurons in the mouse interstitial nucleus of the posterior limb of the anterior commissure (IPAC), a nucleus of the central extended amygdala, encode dietary preference for unhealthy energy-dense foods. Optogenetic activation of IPAC^{Nts} neurons promotes obesogenic behaviors, such as hedonic eating, and modulates food preference. Conversely, acute inhibition of IPAC^{Nts} neurons reduces feeding and decreases hedonic eating. Chronic inactivation of IPAC^{Nts} neurons recapitulates these effects, reduces preference for sweet, non-caloric tastants and, furthermore, enhances locomotion and energy expenditure; as a result, mice display long-term weight loss and improved metabolic health and are protected from obesity. Thus, the activity of a single neuronal population bidirectionally regulates energy homeostasis. Our findings could lead to new therapeutic strategies to prevent and treat obesity.

The prevalence of obesity is increasing worldwide. Although genetic predisposition certainly plays a role, obesity is mostly a consequence of poor dietary choices, maladaptive eating behavior, such as hedonic eating (that is, eating in the absence of hunger), and lack of physical activity¹.

Palatable foods, especially those rich in sugars and fats, are often preferred to healthier alternatives. A highly palatable food's sight, smell and taste (that is, its hedonic properties) can outweigh homeostatic energy balance regulation and the circuits regulating satiety^{2,3} and induce feeding in the absence of an actual energy deficit⁴. Although poor dietary choice is a major cause of obesity, our understanding of how food preference is established is far from complete.

Palatability drives maladaptive eating behavior, such as hedonic and binge eating, which can lead to rapid weight gain. Some schools of thought propose that homeostatic regulatory systems 'defend' a genetically predetermined body weight set point⁵. This regulation is, however, unbalanced, as it seems to be permissive to weight gain. Efforts to lose excess weight by introducing caloric restriction and exercise routines are fiercely counterbalanced by metabolic adaptations that tend to restore the preintervention body weight⁶, making current therapeutic efforts insufficient to stem the tide of obesity.

Despite recognition that energy intake and expenditure are tightly linked components of weight regulation⁷, most research has focused

¹Cold Spring Harbor Laboratory, Cold Spring Harbor, NY, USA. ²School of Biological Sciences, Cold Spring Harbor Laboratory, Cold Spring Harbor, NY, USA. ³Ruprecht Karls University Heidelberg, Heidelberg, Germany. ⁴Northwell Health Cancer Institute, Northwell Health, New Hyde Park, New York, USA. ⁵Present address: Department of Neuroscience, Karolinska Institutet, Stockholm, Sweden. ⁶These authors contributed equally: Alberto Corona, Sara Boyle. ✉e-mail: alessandro.furlan@ki.se; bli@cshl.edu

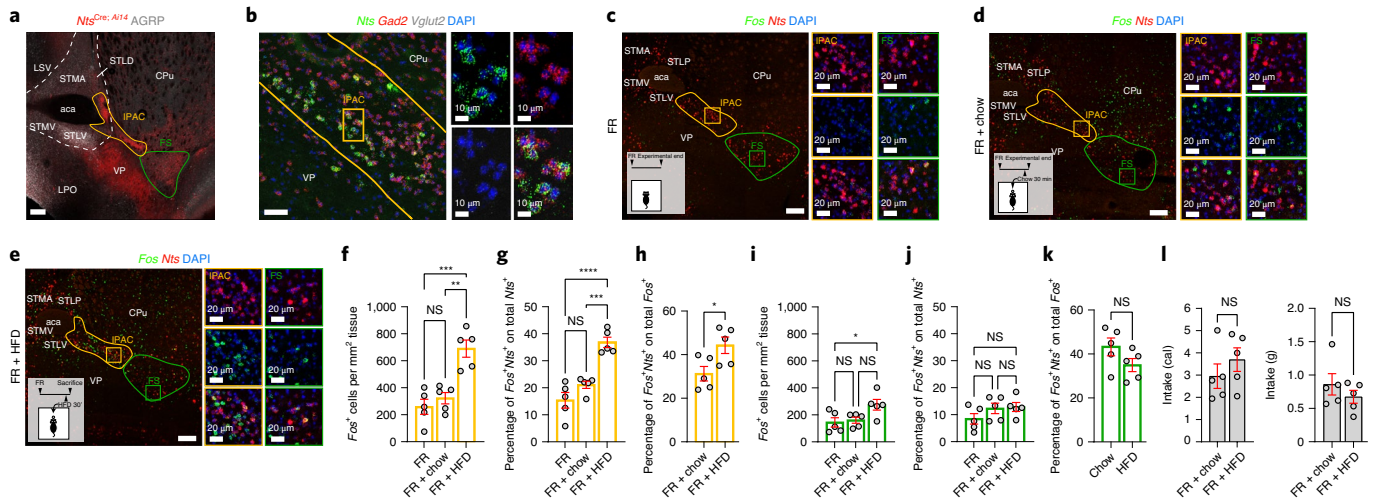


Fig. 1 | IPAC^{Nts} neurons are activated by palatable food in vivo.

a, A coronal brain section containing the IPAC (yellow) and the FS (green) from a representative *Nts^{Cre}; Ai14* mouse; scale bar, 200 μ m; STLV/STLD, ventral/dorsal lateral division of the BNST; STMA/STMV, anterior medial/ventral division; CPu, caudate putamen; LSV, lateral septum; LPO, lateral preoptic area; aca, anterior commissure. **b**, A representative image of IPAC tissue stained for *Nts*, *Gad2* and *Slc17a6* (*Vglut2*). DAPI labels the cell nuclei; scale bar, 50 μ m. **c–e**, Representative images of IPAC tissue stained for *Fos* and *Nts* from FR mice (**c**), FR + chow mice (**d**) and FR + HFD mice (**e**). DAPI labels the cell nuclei; scale bar, 200 μ m; STLP, posterior lateral division of the BNST. **f–k**, Quantification of **c–e**

in the IPAC (**f–h**; yellow) and FS (**i–k**; green); $n = 5$ mice in each group; $F_{2,12} = 18.16$, $P = 0.0002$ (**f**); $F_{2,12} = 26.61$, $P < 0.0001$ (**g**); $P = 0.0318$ (**h**); $F_{2,12} = 4.619$, $P = 0.0325$ (**i**); $F_{2,12} = 1.660$, $P = 0.2309$ (**j**); $P = 0.1393$ (**k**). Data in **f, g, i** and **j** were analyzed by one-way analysis of variance (ANOVA) followed by a Sidak multiple comparisons test; **** $P < 0.0001$, *** $P < 0.001$, ** $P < 0.01$, * $P < 0.05$, $P > 0.05$ (not significant) (NS). Data in **h** and **k** were analyzed by unpaired *t*-test. **l**, Quantification of energy intake (calories; left) and food intake (grams; right) in mice fed chow and a HFD; left, $P = 0.3578$ (NS); right, $P = 0.3450$ (NS). Data were analyzed by unpaired *t*-test and are presented as mean \pm s.e.m.

on identifying the brain circuits that contribute to feeding⁸, whereas those regulating energy expenditure via behavior (for example, locomotion) and metabolic thermogenesis have received less attention. Identification of the brain networks that shape dietary choice and the control of these behaviors and physiological adaptations is crucial to devise new therapeutic approaches.

The interstitial nucleus of the posterior limb of the anterior commissure (IPAC) is a major structure of the extended amygdala (EA)⁹. IPAC neurons are activated by innate or learned gustatory stimuli^{10,11}, and they receive dense projections from the insular cortex, a hedonic hot spot¹². However, to date, no study has addressed the IPAC's role in energy homeostasis. Here, we uncover a critical role for neurotensin-expressing neurons within the IPAC in establishing dietary choice and orchestrating behaviors that impact metabolic health.

Results

IPAC^{Nts} neurons are specifically activated by palatable food

To verify *Nts* expression in the IPAC, we bred *Nts^{Cre}; Ai14* mice, in which *Nts*-expressing (*Nts⁺*) neurons express the red fluorescent protein tdTomato¹³. The expression pattern of Cre recapitulated that of endogenous *Nts* in the IPAC of *Nts^{Cre}* mice (Supplementary Fig. 1a), thus validating the fidelity of this line. We took advantage of *Ai14* expression, in combination with agouti-related protein (AgRP) immunostaining, to outline the borders of the IPAC and the fundus striati (FS)¹⁴ and to distinguish these areas from the bed nuclei of the stria terminalis (BNST; whose neurons are innervated by hypothalamic AgRP⁺ neurons¹⁵) and the ventral pallidum (VP). We found that dense *Nts⁺* cells form a narrow stripe in the IPAC, which merge with the sparser *Nts⁺* cells in the FS and the lateral nuclei of the BNST (Fig. 1a and Supplementary Fig. 1b,c). No *Nts⁺* neurons were observed in the VP, although it is rich in axon fibers originating from *Nts⁺* neurons (Fig. 1a and Supplementary Fig. 1b,c). Single-molecule fluorescence in situ hybridization (smFISH) confirmed *Nts* expression in the IPAC complex and its near absence in

nearby striatal and VP territories. Virtually all *Nts⁺* neurons in the IPAC were GABAergic (Fig. 1b).

Food restriction creates a negative energy balance and leads to the activation of homeostatic circuits that regulate energy intake to restore the balance¹⁶. To test whether IPAC^{Nts} or FS^{Nts} neurons are involved in this process, we analyzed the expression of *Fos*, a molecular marker that is a proxy for neuronal activation, in food-restricted (FR) mice (Fig. 1c), mice refed with regular chow (FR + chow; Fig. 1d) or mice refed a high-fat diet (HFD; FR + HFD; Fig. 1e and Methods). A HFD, but not chow, induced a significant increase in *Fos* expression in both IPAC and FS regions (Fig. 1f,i). Interestingly, a HFD increased *Fos* expression in *Nts⁺* neurons of the IPAC but not the FS (Fig. 1g,j and Supplementary Fig. 1d,e), implicating *Nts* as a potential marker to genetically access this brain region and its role in energy homeostasis. Conversely, we found an increased representation of *Nts⁺* neurons within *Fos⁺* neurons in the IPAC but not FS when mice were fed a HFD (Fig. 1h,k). Of note, mice fed chow or a HFD had similar food intake (Fig. 1l). These results suggest that IPAC^{Nts} neurons are activated preferentially by the consumption of palatable food but not necessarily by an energy deficit or by motor programs underlying food consumption.

IPAC^{Nts} neurons encode food preference

Our understanding of how food preference is established is incomplete. Based on our *Fos* data, we reasoned that IPAC^{Nts} neurons could encode food palatability and therefore diet preference. To test this hypothesis, we sought to monitor the in vivo activity of these neurons in behaving mice consuming diets with differing palatability. We first labeled these neurons with the genetically encoded calcium indicator GCaMP6f¹⁷ by injecting the IPAC of *Nts^{Cre}* mice with an adeno-associated virus (AAV) expressing GCaMP6f in a Cre-dependent manner and implanted an optical fiber into the same location (Fig. 2a and Extended Data Fig. 1a). This strategy enabled us to record IPAC^{Nts} neuron activity in vivo in behaving animals.

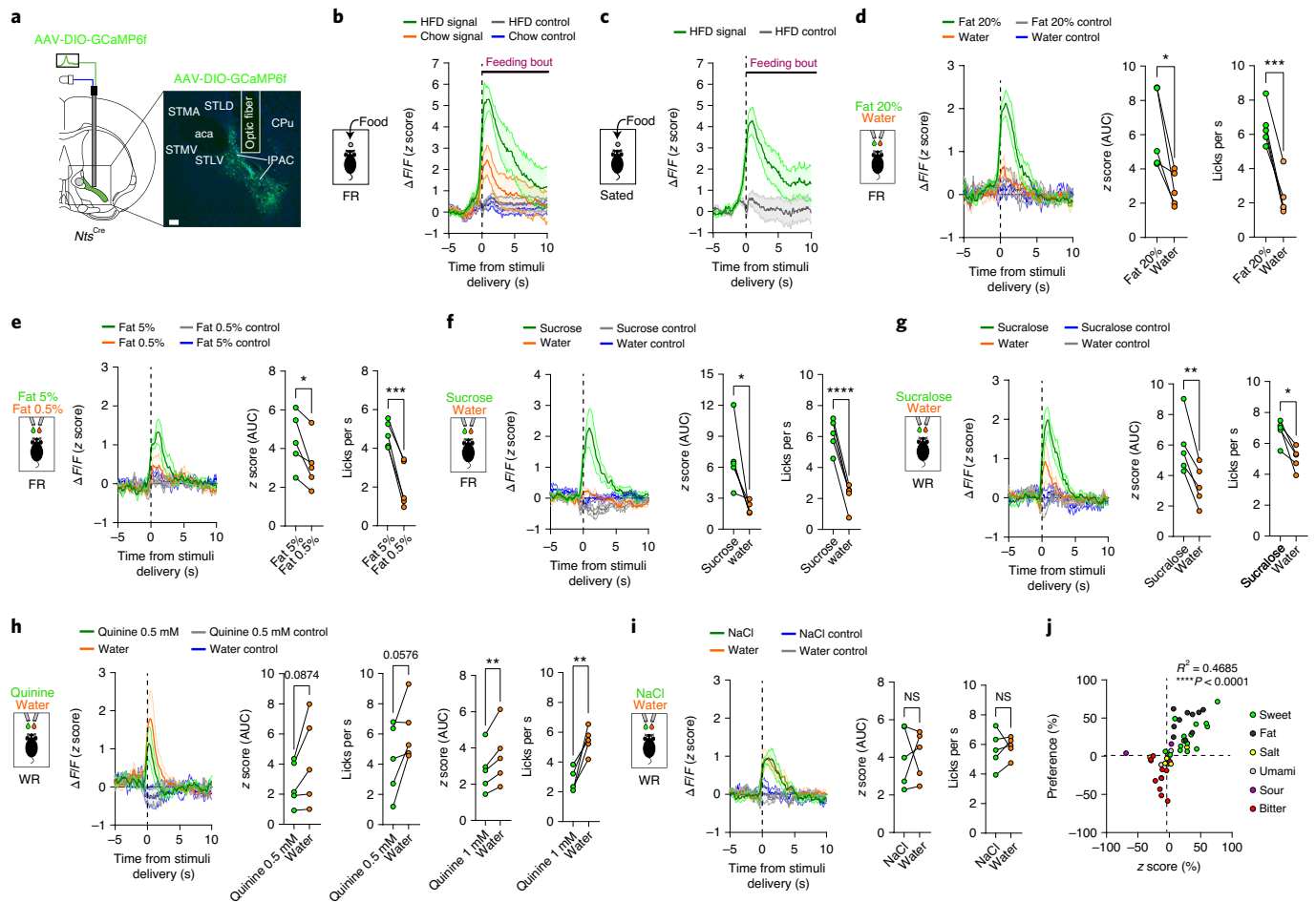


Fig. 2 | IPAC^{NTS} neurons encode the hedonic value of a tastant. **a**, Representative histological image; scale bar, 100 μ m. **b**, FR mice presented with a HFD (green trace) or chow (orange trace); feeding bouts, 10 s; dashed line, stimulus presentation; gray/blue traces, isosbestic controls; $n = 5$ mice. **c**, Mice sated on chow presented with a HFD; feeding bouts, 10 s; dashed line, stimulus presentation; gray trace, isosbestic control; $n = 7$ mice. **d–i**, FR mice (**d–f**) and WR mice (**g–i**) were given equal volumes of liquids in the same session. Left, average GCaMP6f signals from IPAC^{NTS} neurons. The dashed lines indicate the stimulus presentation (first lick). Center, area under the curve (AUC) of GCaMP6f signals. Right, licking behavior (behavior) of mice. AUC and licking behavior were measured in 3-s windows following the first lick. Gray/blue traces indicate isosbestic controls. Data were analyzed by paired t -tests; $n = 5$ mice per group. **d**, Intralipid (fat 20%, green trace) or water (orange trace); AUC, $*P = 0.0234$;

behavior, $***P = 0.0002$. **e**, Intralipid 5% (fat 5%, green trace) or Intralipid 0.5% (fat 0.5%, orange trace); AUC, $*P = 0.0309$; behavior, $***P = 0.0008$. **f**, Sucrose (green trace) or water (orange trace); AUC, $*P = 0.0388$; behavior, $****P < 0.0001$. **g**, Sucralose (green trace) or water (orange trace); AUC, $**P = 0.0049$; behavior: $*P = 0.0109$. **h**, Quinine (green trace) or water (orange trace); AUC quinine 0.5 mM versus water, $P = 0.0874$; AUC quinine 1 mM versus water, $**P = 0.0095$; behavior quinine 0.5 mM versus water, $P = 0.0576$; behavior quinine 1 mM versus water, $**P = 0.0057$. **i**, NaCl (green trace) or water (orange trace); AUC, $P = 0.9292$ (NS); behavior, $P = 0.7136$ (NS). **j**, Correlation between the amplitude of GCaMP6f signals from IPAC^{NTS} neurons for a tastant (z score percent, x axis) and licking behavioral preference for such tastant; $****P < 0.0001$ and $R^2 = 0.4685$. Data were analyzed by Pearson correlation test and are presented as mean \pm s.e.m.

We started by testing the response of IPAC^{NTS} neurons to chow and a HFD in FR conditions. When these diets were presented simultaneously, mice strongly preferred a HFD to chow (Extended Data Fig. 1b). For this reason, for our testing, chow and HFD diets were presented to mice on consecutive days in a randomized order (Methods). In hungry mice, we found that the amplitude of the response of IPAC^{NTS} neurons was higher for a HFD than for chow (Fig. 2b). To test whether IPAC^{NTS} neurons are activated by palatable food when sated, we presented sated mice with a HFD. Again, IPAC^{NTS} neurons were strongly activated (Fig. 2c). Importantly, because the feeding bout duration was similar (and uninterrupted) for both diets (that is, 10 s; Fig. 2b,c), we conclude that the difference in this response is not due to motor behaviors or a satiety signal but rather the palatability of the stimulus. Because the most palatable foods are in general the most preferred and sought after (Extended Data Fig. 1b), we hypothesized a role for IPAC^{NTS} in encoding food preference and direct consummatory behaviors.

To test this, we aimed to deliver two stimuli in the same session, therefore creating the condition for a preference to be established. Because taste is one of the most salient stimuli regulating food preference and intake, we presented FR mice expressing GCaMP6f in IPAC^{NTS} neurons with equal volumes of tastants with clearly distinct palatability delivered via two spouts (Methods and Extended Data Fig. 1c,d). We presented a liquid fat diet (Intralipid) that is commonly used as liquid food¹⁸ and is highly palatable. We found that, in line with behavioral preferences of the mice (Extended Data Fig. 1e), immediately following ingestion, IPAC^{NTS} neurons were more robustly activated by fat than by water (Fig. 2d) in a concentration-dependent manner (Fig. 2e). Similarly, IPAC^{NTS} neurons of FR mice were more robustly activated by sucrose than by water (Fig. 2f) and by sucrose than by sucralose (a sweet, thus palatable, but non-caloric sugar analog; Extended Data Fig. 1f). These results further indicate that IPAC^{NTS} neurons respond to palatable stimuli and that their activity is scaled by the palatability of the

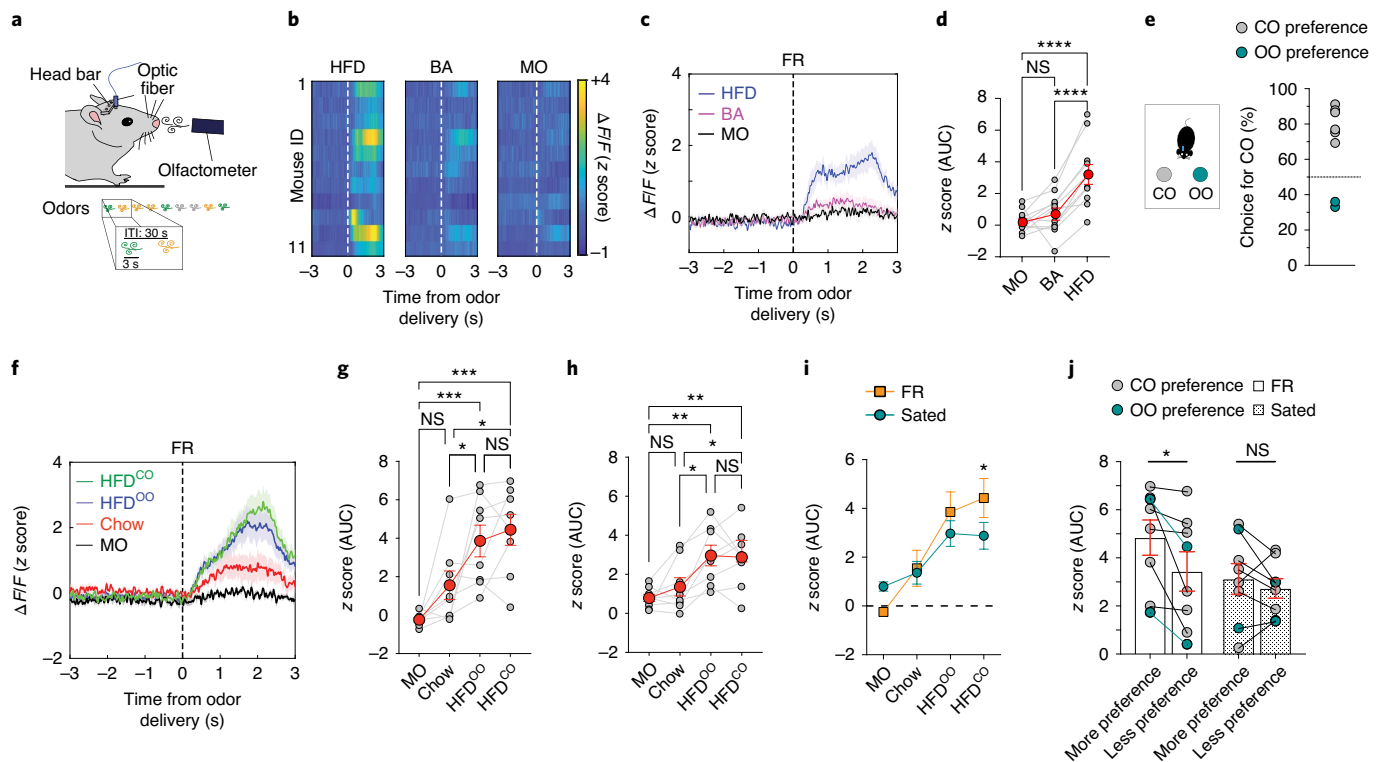


Fig. 3 | IPAC^{Nts} neurons encode the hedonic value of an odor. **a**, A schematic of the experimental setup to test odor preference; ITI, inter-trial interval. **b**, Heat maps of average GCaMP6f responses of IPAC^{Nts} neurons in individual mice; dashed line, stimulus presentation. **c**, Average GCaMP6f signals from IPAC^{Nts} neurons in FR mice in response to HFD, BA and MO; dashed line, stimulus presentation. **d**, AUC of the responses in individual mice measured in a 3-s window following odor presentation; $n = 11$ mice, $F_{2,20} = 25.64$, $P < 0.0001$, **** $P < 0.0001$. Data were analyzed by one-way repeated-measures (RM) ANOVA followed by a Holm–Sidak test. **e**, Mouse behavioral preference for CO-based (HFD^{CO}) and OO-based (HFD^{OO}) HFDs. **f**, Average GCaMP6f signals from IPAC^{Nts} neurons of mice in **e** under food restriction aligned to odor presentation (dashed line). **g**, AUC of the responses of mice in **e** and **f** under food restriction in a 3-s window following odor presentation; dashed line, stimulus presentation; $n = 8$

mice, $F_{3,21} = 11.96$, $P < 0.0001$; NS, $P > 0.05$, * $P < 0.05$, **** $P < 0.001$. Data were analyzed by one-way RM ANOVA followed by a Holm–Sidak test. **h**, AUC of the responses of mice in **e**, sated, in a 3-s window following odor presentation; $n = 8$ mice, $F_{3,21} = 8.546$, $P = 0.0007$; NS, $P > 0.05$, * $P < 0.05$, ** $P < 0.01$. Data were analyzed by one-way RM ANOVA followed by a Holm–Sidak multiple comparisons test. **i**, Average responses of IPAC^{Nts} neurons in **g** and **h** are replotted for visual inspection; interaction effect: $F_{3,21} = 5.394$, $P = 0.0065$, * $P < 0.05$. Data were analyzed by two-way RM ANOVA followed by a Holm–Sidak test. **j**, IPAC^{Nts} neurons responded more to the preferred than to the non-preferred HFD in FR mice (left) but not sated mice (right); $n = 8$ mice, $F_{1,7} = 8.769$, $P = 0.0211$, NS, $P > 0.05$, * $P < 0.05$. Data were analyzed by two-way RM ANOVA followed by a Holm–Sidak test. Data are presented as mean \pm s.e.m.

stimuli. To investigate whether the activity of IPAC^{Nts} neurons encode subtle changes in palatability, we water restricted mice and tested them with an array of non-caloric tastants (representing sweet, bitter, salt, umami and sour) or water (Fig. 2g–i and Extended Data Fig. 1g,h).

If IPAC^{Nts} neurons encode the palatability of a taste stimulus, then we would expect appetitive tastants (for example, sucralose (sweet)) to evoke a higher response and an aversive tastant (for example, quinine, a bitter, unpalatable, non-caloric compound) to effectively reduce the amplitude of IPAC^{Nts} neuron firing compared to water. Indeed, the IPAC^{Nts} neurons of water-restricted (WR) mice were more robustly activated by sucralose than by water (Fig. 2g) and more by water than by quinine (Fig. 2h). Ingestion of salty (Fig. 2i), umami and sour tastants (Extended Data Fig. 1g,h) did not elicit a significantly different response compared to water. Analysis of the licking behavior, a proxy for preference¹⁹, showed that mice, irrespective of the inner state (hungry or thirsty) licked the spout delivering the preferred tastants more vigorously (Fig. 2d–i and Extended Data Fig. 1f–h). Analysis of the relationship between the responses of IPAC^{Nts} neurons and the licking behavior showed that in the vast majority of cases (90%), these variables were not correlated (Methods and Supplementary Fig. 2). However, we found a strong correlation between the amplitude of the neural response for the preferred tastant and the behavioral preference for that tastant

(Fig. 2j and Methods). Altogether, these results suggest that IPAC^{Nts} neuron activity represents tastant palatability and dietary preference.

In addition to taste, the smell of a food also has a major impact on its palatability²⁰, which undoubtedly influences feeding choices^{21,22}. To examine whether IPAC^{Nts} neurons respond to food-related smells, we measured their in vivo responses in head-fixed mice (Fig. 3a) presented with food-related odors from a palatable HFD dissolved in mineral oil (MO), unpalatable butyric acid (BA; typically found in spoiled food and responsible for its rotten smell) in MO and MO alone as the vehicle control (Methods). Notably, we found that IPAC^{Nts} neurons were strongly activated by a HFD but not by BA or MO (Fig. 3b–d). These results suggest that IPAC^{Nts} neurons respond to appetitive but not aversive food-related sensory cues.

To determine whether IPAC^{Nts} neuron activity encodes more subtle dietary preference, we presented mice with two pairs of rewarding HFDs with identical nutritional value: (1) HFD^{CO} (coconut-flavored) and HFD^{OO} (olive oil-flavored) diets and (2) white chocolate (WCh) and dark chocolate (DCh), which are among the popular energy-dense foods causing obesity in humans. Before testing, mice were presented with each diet pair simultaneously in their home cage to ensure familiarity (Methods). All mice showed a clear preference for either HFD^{CO} or HFD^{OO} (Fig. 3e) and for WCh over DCh (data not shown). Once the food preference was established, we head fixed these mice to the

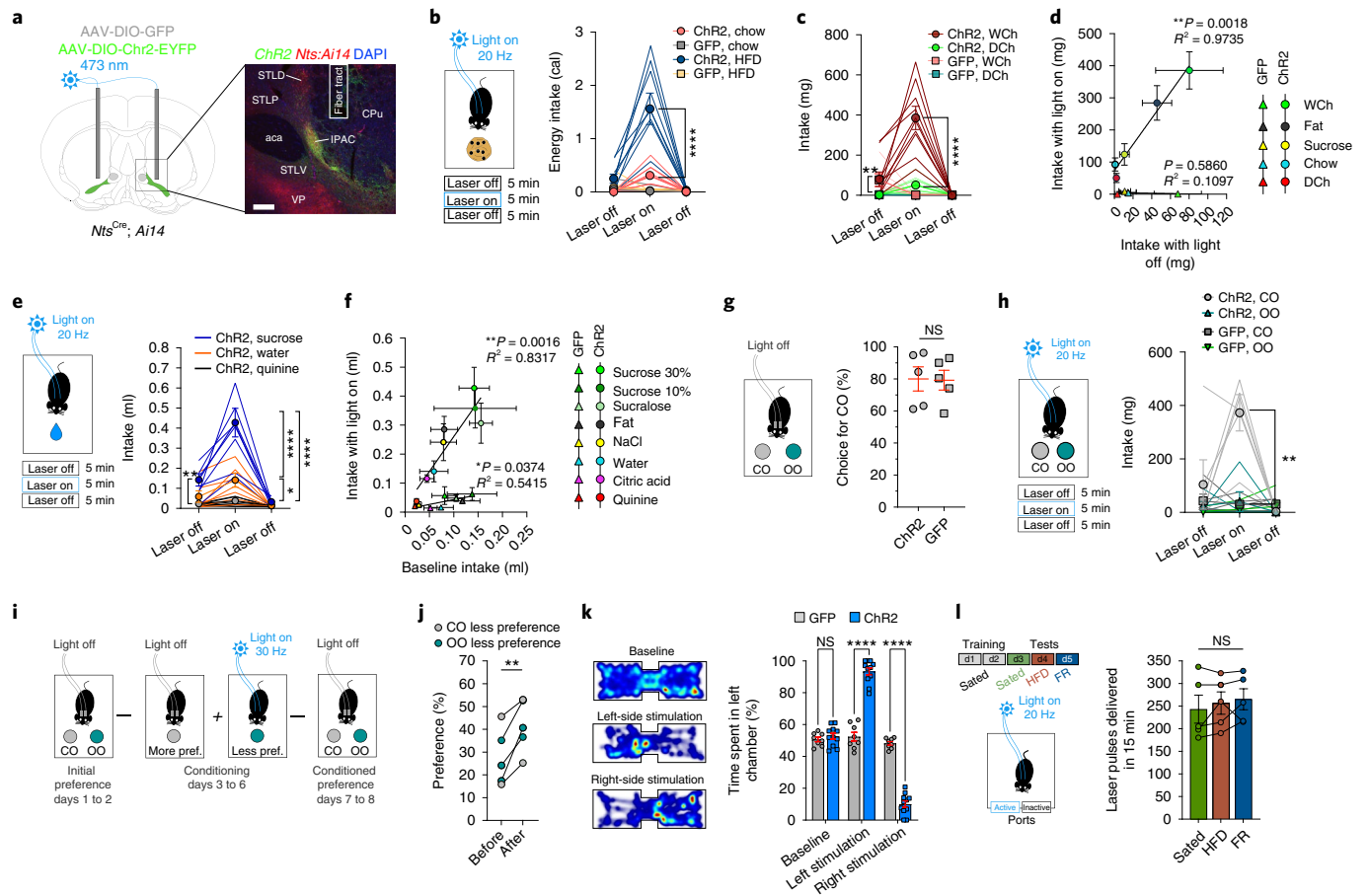


Fig. 4 | Activation of IPAC^{Nts} neurons regulates dietary choices.

a, Representative histological image; scale bar, 200 μm . **b**, Left, schematic of the paradigm; right, intake of fed chow or a HFD; ChR2 ($n = 9$), interaction effect: $F_{2,16} = 17.75$, $P < 0.0001$, **** $P < 0.0001$; GFP ($n = 8$), group effect: $F_{1,7} = 9.164$, $P = 0.0192$, $P > 0.05$ (NS). Data were analyzed by two-way RM ANOVA followed by a Sidak test. **c**, Intake of mice fed WCh or DCh; ChR2 ($n = 9$), $F_{2,16} = 19.12$, $P < 0.0001$, **** $P < 0.0001$; GFP ($n = 6$), $F_{2,10} = 5.6$, $P = 0.0234$, ** $P < 0.001$. Data were analyzed by two-way RM ANOVA followed by a Sidak test. **d**, Correlation between food intake at baseline and during photostimulation; ChR2 ($n = 9$), ** $P = 0.0018$; GFP (chow, sucrose, HFD, WCh; $n = 8$; DCh; $n = 6$), $P = 0.5860$ (NS). Data were analyzed by Pearson correlation test. **e**, Liquid intake of ChR2 mice ($n = 7$); interaction effect: $F_{4,24} = 14.90$, $P < 0.0001$, * $P < 0.05$, **** $P < 0.0001$, ** $P < 0.001$ between sucrose and quinine during the first laser-off period. Data were analyzed by two-way RM ANOVA followed by a Tukey test. **f**, Correlation between liquid intake at baseline and during photostimulation; ChR2 ($n = 7$), ** $P = 0.0016$;

GFP ($n = 5$), * $P = 0.0374$. Data were analyzed by Pearson correlation test. **g**, Preference for HFD^{CO} over HFD^{OO} with the light off; $n = 5$ mice per group, $P = 0.9385$ (NS). Data were analyzed by unpaired t -test. **h**, Intake of mice (in grams) of HFD^{CO} and HFD^{OO} with the light on; ChR2 ($n = 5$), interaction effect: $F_{2,8} = 9.443$, $P = 0.0078$, ** $P < 0.01$; GFP ($n = 5$), interaction effect: $F_{2,8} = 0.9049$, $P = 0.4423$. Data were analyzed by two-way RM ANOVA followed by a Sidak test. **i**, Paradigm for conditional flavor preference (pref.). **j**, Effects of light delivery on food preference; $n = 5$ mice per group, ** $P = 0.0082$. Data were analyzed by paired t -test. **k**, Left, heat maps of a representative mouse in the RTPP/A task; right, preference of ChR2 ($n = 11$) and GFP ($n = 8$) mice for the left chamber; interaction effect: $F_{2,34} = 208.5$, $P < 0.0001$, **** $P < 0.0001$, $P > 0.05$ (NS). Data were analyzed by two-way RM ANOVA followed by a Sidak test. **l**, Self-stimulation behavior of ChR2 mice ($n = 5$) under different homeostatic states; d, day; $F_{2,8} = 1.463$, $P = 0.2875$ (NS). Data were analyzed by one-way ANOVA and are presented as mean \pm s.e.m.

olfactometer and presented them with the following odors: (1) HFD^{CO}, HFD^{OO}, chow and MO (Fig. 3f–h and Extended Data Fig. 2a) and (2) WCh, DCh, chow and MO (Extended Data Fig. 2b–f). We found that irrespective of the metabolic state of the animal (FR or sated), IPAC^{Nts} neurons showed higher responses to energy-dense foods (HFDs and chocolate) than to plain chow (Fig. 3f–h and Extended Data Fig. 2c–f), although their response was larger when mice were FR, suggesting odor alliesthesia²³ (Fig. 3i). Notably, when the pretest idiosyncratic preferences of individual mice for one of the two HFDs were considered (Fig. 3e), IPAC^{Nts} neuron responses were larger for the odor of the favored diet irrespective of it being CO or OO flavored (Fig. 3j). These data suggest that the activity of IPAC^{Nts} neurons encodes preference independently of the nutritional value of the stimulus. As sensory perception of palatable diets induces IPAC^{Nts} neuron activation even in the absence of hunger, we hypothesized that activation of IPAC^{Nts} neurons might drive maladaptive eating behaviors (for example, hedonic feeding).

Activation of IPAC^{Nts} neurons promotes hedonic feeding

To assess whether activation of IPAC^{Nts} neurons could result in overfeeding, we selectively activated these neurons in sated mice with optogenetics. For this purpose, we bilaterally injected the IPAC of *Nts*^{Cre} mice with an AAV expressing the light-gated cation channel channelrhodopsin (ChR2) or green fluorescent protein (GFP; as a control) in a Cre-dependent manner. We implanted optical fibers over the infected areas for light delivery (Fig. 4a and Extended Data Fig. 3a). Following recovery from surgery and viral expression, sated mice received pellets of differing palatability, either on consecutive days or simultaneously (Methods). During each food presentation, pulses of blue light (20 Hz, 7–10 mW, 5-min duration) were delivered into the IPAC, preceded and followed by an additional 5 min with no light (Fig. 4b and Methods). We found that photostimulation in the ChR2 mice, but not in the GFP mice, generally increased intake for all diets (Extended Data Fig. 3b) and liquids (Fig. 4e,f). The effect was larger for the more palatable HFD and WCh than for chow and DCh (Fig. 4b,c),

respectively, and for liquid solutions of sucrose than for water or quinine (Fig. 4e and Extended Data Fig. 3g). Consistently, the number and length of feeding bouts were also increased by photostimulation (Extended Data Fig. 3d,e). Of note, IPAC^{Nts} neuron activation did not induce any feeding on an inedible eraser, suggesting that the effect is food specific, although it enhanced gnawing (Extended Data Fig. 3c and Methods). We found a correlation between the baseline intake (that is, the mouse preference for a diet, a function of its palatability) and the activation-induced intake of the different diets and liquids (Fig. 4d,f). Next, we repeated the above experiments with two additional pairs of isocaloric foods: (1) plain chow and chow flavored with quinine (Extended Data Fig. 3f) and (2) HFD^{CO} and HFD^{OO} (Fig. 4g,h) in sated mice. Mice were habituated to HFD^{CO} and HFD^{OO} diets before the start of the experiment, and all mice showed a clear preference for HFD^{CO} (Fig. 4g). We found that in both cases, activation of IPAC^{Nts} neurons increased the intake of the more palatable food to a higher degree than the less palatable counterpart in the pair (Fig. 4h and Extended Data Fig. 3f). Next, we sought to investigate whether photostimulation of IPAC^{Nts} neurons might condition flavor preference. After the baseline preference was established, we performed conditioning (Methods) by pairing the less preferred diet with light delivery. After conditioning, we found that, although in most cases conditioning did not completely reverse the original preference, photostimulation increased the preference for the less preferred diet (Fig. 4i,j).

Activation of IPAC^{Nts} neurons is positively reinforcing

Activation of IPAC^{Nts} neurons effectively supports self-stimulation (Extended Data Fig. 3h and Methods) and induces place preference in a real-time place preference or aversion (RTPP/A) assay (Fig. 4k and Methods), suggesting that it is intrinsically rewarding. To determine whether IPAC^{Nts} neuron self-stimulation was independent of the homeostatic state of the animal²⁴, we repeated the self-stimulation experiment in mice in neutral (that is, sated), positive (that is, overfed) and negative (that is, FR) energy balance (Methods). We found that self-stimulation was independent of the internal state of the animal (Fig. 4l). Notably, we found that activation of IPAC^{Nts} neurons caused a significant reduction in movement in both the RTPP/A assay and in an open field (OF) test (Extended Data Fig. 3i,j and Methods).

Together, these data indicate that activity of IPAC^{Nts} neurons drives feeding proportionate to the palatability of the food and modulates intake and preference, thereby shaping dietary preferences.

Inhibition of IPAC^{Nts} neurons impairs feeding behavior

We then hypothesized that inhibition of IPAC^{Nts} neurons could have opposite effects on energy intake (that is, feeding). To investigate this, we selectively and transiently inhibited these neurons in sated mice with chemogenetics. For this purpose, we bilaterally injected the IPAC of *Nts*^{Cre} mice with an AAV expressing κ -opioid-derived DREADD (KORD)²⁵ or mCherry (as a control) in a Cre-dependent manner (Methods and Fig. 5a). To test whether acute inhibition of IPAC^{Nts} neurons impairs homeostatic feeding, we food restricted control and experimental mice overnight (O/N). The following day, mice were injected with either SalvinorinB (SalB; a selective KORD DREADD activator²⁵) or vehicle dimethyl sulfoxide (DMSO; Methods). Chow was reintroduced to the mice 20 min later for testing. We found that SalB (but not DMSO) injections reduced refeeding in KORD but not mCherry mice (Fig. 5b). Next, we tested whether inhibition of IPAC^{Nts} neurons would reduce feeding on a palatable HFD in mice sated on chow. We found that SalB (but not DMSO) injection decreased feeding on a HFD in KORD but not mCherry sated mice (Fig. 5c). Of note, no significant change in drinking behavior or locomotor activity (Fig. 5d,e) was observed, suggesting a specific role for these neurons in the regulation of feeding behavior.

Inactivation of IPAC^{Nts} neurons promotes weight loss

The reduction of feeding in KORD mice treated with SalB could have important implications for preventing obesity. However, due to the

transient nature of the inhibition, this effect is short lived (Extended Data Fig. 4a). We hypothesized that a more protracted inhibition of IPAC^{Nts} neurons might reduce feeding on a HFD in the long term and thus delay or prevent obesity onset. To test this, we bilaterally injected the IPAC of *Nts*^{Cre} mice with a Cre-dependent tetanus toxin light chain virus (TeLC mice)²⁶ or a control virus (GFP mice; Fig. 5f and Supplementary Fig. 5b). We confirmed that, in line with our chemogenetic data, inactivation of IPAC^{Nts} neurons impairs homeostatic feeding (Fig. 5g) but not drinking behavior (Fig. 5h). We then monitored behavior and metabolic parameters of TeLC and control mice in metabolic cages (Methods). Although inactivation of IPAC^{Nts} neurons reduced energy intake in refeeding tests (Fig. 5b,g), it did not affect food (chow) or water intake of the TeLC mice when these were freely available (Fig. 5i and Extended Data Fig. 4c). However, when we replaced chow with a HFD, we found that, after 4 d, the TeLC mice ate significantly less HFD than control mice (Fig. 5j). Water intake of TeLC mice was also lower (Extended Data Fig. 4d). Consistently, GFP, but not TeLC, mice dramatically increased their caloric intake (Extended Data Fig. 4f) and likely entered a positive energy balance state (Extended Data Fig. 4g). Indeed, after only 4 d of a HFD, the body weight of the GFP mice was dramatically increased, whereas that of TeLC mice remained stable (Fig. 5k).

We next sought to identify whether the reduction of food intake was due to a deficit in detecting the hedonic or nutritional features of food. We show that transient inhibition of IPAC^{Nts} neurons reduced feeding on a HFD within 30 min from meal initiation (Extended Data Fig. 4b), after gustatory inputs and likely before postingestive conditioning takes place. Therefore, this result suggests a role for IPAC^{Nts} neurons in encoding hedonic stimuli. To further probe this, we tested the preferences of the mice for either sucralose (sweet but non-caloric, therefore not eliciting postingestive effects) or sucrose (sweet and also caloric) over plain water (Extended Data Fig. 4e). Notably, the TeLC mice showed an impaired ability to form a preference for sucralose but not for sucrose.

Our loss-of-function data show that inhibition or inactivation of IPAC^{Nts} neurons reduces overeating of palatable energy-dense diets, thereby protecting from obesity onset (Fig. 5k). We sought to investigate whether inactivation of IPAC^{Nts} neurons could regulate body weight and have beneficial effects on metabolic health.

We noticed that the TeLC group lost weight within 10 d after surgery and subsequently stabilized between day 10 and day 30 (Fig. 6a and Extended Data Fig. 5a), despite food and water being freely available in the home cage. A reduction in body weight is normally caused by an imbalance between energy intake and expenditure. We found that the energy expenditure and locomotion of TeLC mice were higher than those of controls (Fig. 6b–d).

Anxiety and stress-related states can induce hyperactivity²⁷. To determine whether our manipulation induced anxiety-related behaviors, we subjected the TeLC mice and GFP control mice to the elevated-plus maze (EPM) and OF tests. We found no difference between the two groups in measures of anxiety behaviors in rodents (Supplementary Fig. 3).

These data show that prolonged inactivation of IPAC^{Nts} neurons enhances locomotion and energy expenditure, effectively leading mice to achieve long-term weight loss.

Inactivation of IPAC^{Nts} neurons promotes metabolic health

We sought to investigate whether increased locomotion induced by inhibition of IPAC^{Nts} neurons could have beneficial effects on mouse metabolism. We found that the TeLC group had markedly higher volume of oxygen inhaled (oxygen consumption; VO₂), higher carbon dioxide released (carbon dioxide production; VCO₂) and a lower respiratory exchange ratio (RER) than controls (Fig. 6e,f and Extended Data Fig. 5b–e), suggesting that in TeLC mice, the oxidation rate of lipids was enhanced. These behavioral and metabolic changes protected mice from obesity. After 6 weeks under a diet-induced obesity (DIO)

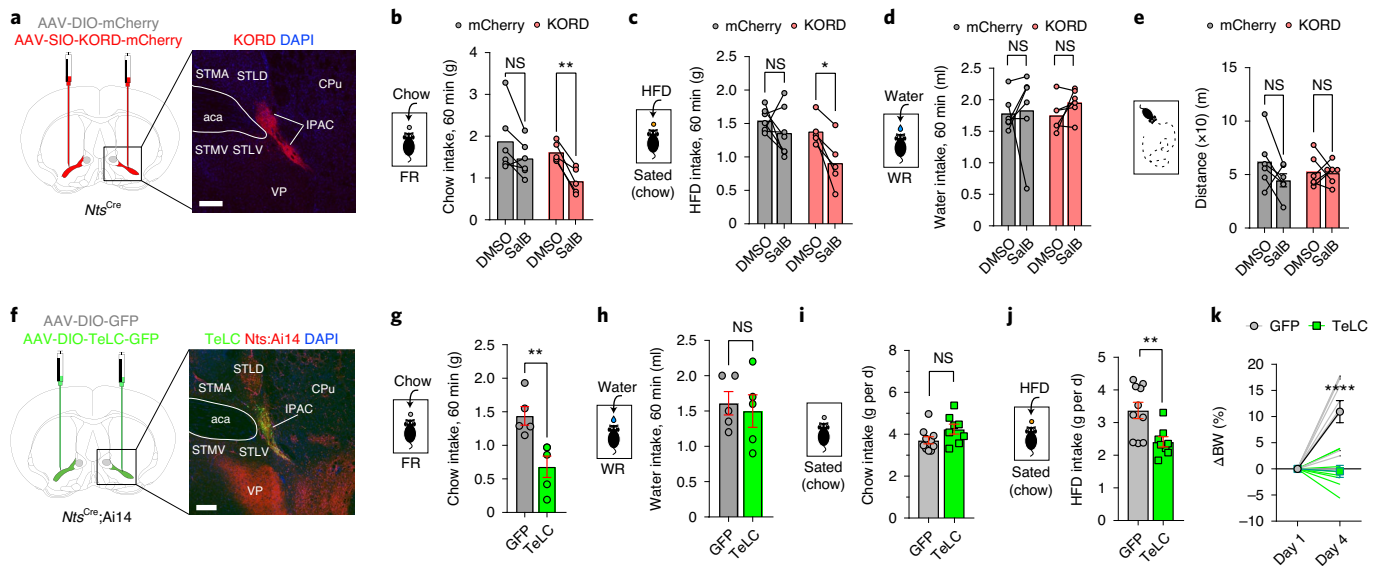


Fig. 5 | Inhibition and inactivation of IPAC^{Nts} neurons both disrupt feeding.

a, An image showing KORD expression in IPAC^{Nts} neurons in a representative *Nts^{Cre}* mouse; scale bar 200 μ m. **b**, Chow intake over a 1-h period in FR *Nts^{Cre}* mice; mCherry mice, $n = 6$; KORD mice, $n = 5$; mCherry DMSO versus SalB: $P = 0.0785$ (NS); KORD DMSO versus SalB: $**P = 0.0031$. Data were analyzed by paired *t*-test. **c**, HFD intake over a 1-h period in sated *Nts^{Cre}* mice; mCherry mice, $n = 7$; KORD mice, $n = 5$; mCherry DMSO versus SalB: $P = 0.3194$ (NS); KORD DMSO versus SalB: $*P = 0.0141$. Data were analyzed by paired *t*-test. **d**, Water intake over a 1-h period in WR *Nts^{Cre}* mice; mCherry mice, $n = 6$; KORD mice, $n = 6$; mCherry DMSO versus SalB: $P = 0.8725$ (NS); KORD DMSO versus SalB: $P = 0.1672$ (NS). Data were analyzed by paired *t*-test. **e**, Locomotor activity over a 1-h period in sated *Nts^{Cre}* mice; mCherry mice, $n = 6$; KORD mice, $n = 6$; mCherry DMSO versus SalB: $P = 0.1433$ (NS); KORD DMSO versus SalB: $P = 0.8981$ (NS). Data were analyzed

by paired *t*-test. **f**, An image showing TeLC expression in IPAC^{Nts} neurons in a representative *Nts^{Cre}* mouse; scale bar, 200 μ m. **g**, Chow intake over a 1-h period in FR *Nts^{Cre}* mice; GFP mice, $n = 5$; TeLC mice, $n = 5$; $**P = 0.0071$. Data were analyzed by unpaired *t*-test. **h**, Water intake over a 1-h period in WR *Nts^{Cre}* mice; GFP mice, $n = 5$; TeLC mice, $n = 5$; $P = 0.7085$ (NS). Data were analyzed by unpaired *t*-test. **i**, Daily chow intake over a 72-h period in *Nts^{Cre}* mice; GFP mice, $n = 10$; TeLC mice, $n = 8$; $P = 0.0785$ (NS). Data were analyzed by unpaired *t*-test. **j**, Daily HFD intake over a 96-h period in *Nts^{Cre}* mice; GFP mice, $n = 10$; TeLC mice, $n = 8$; $**P = 0.0073$. Data were analyzed by unpaired *t*-test. **k**, Acute changes in body weight (BW) following 4 d of HFD; interaction effect: $F_{1,16} = 19.45$, $P = 0.0004$, $****P < 0.0001$. Data were analyzed by two-way RM ANOVA followed by a Sidak multiple comparisons test. Data are presented as mean \pm s.e.m.

paradigm, the GFP mice became obese, but, in stark contrast, the TeLC mice remained lean (Fig. 6g,h). We sought to identify potential mechanisms protecting the TeLC mice from developing obesity. In mice that switch to a HFD, lipid oxidation is not immediately adjusted to match HFD over-intake, resulting in positive energy balance²⁸. Interestingly, the TeLC mice displayed a more rapid adaptation to the diet switch than control mice, suggesting a higher lipid oxidation rate (Fig. 6i). Further, we found that even when fed a HFD, these mice displayed markedly elevated energy expenditure, VO_2 , VCO_2 and locomotion (Extended Data Fig. 5f–i). Because lipid oxidation is enhanced in mice with access to a running wheel²⁹, it is likely that the enhanced lipid oxidation rate of the TeLC mice is due to their enhanced movement, which partially explains their resistance to weight gain.

Obesity is often comorbid with life-threatening conditions, such as diabetes. We tested whether inhibition of IPAC^{Nts} neurons could improve glucose homeostasis. Indeed, we found that blood glucose levels were significantly lower in the TeLC mice than in GFP mice in a glucose tolerance test (GTT) and in an insulin tolerance test (ITT; Fig. 6j,k and Methods). Thus, inhibition of IPAC^{Nts} neurons preserves glucose homeostasis in mice fed a HFD.

Inactivation of IPAC^{Nts} neurons protected TeLC mice from weight gain in the long term. At endpoint, the body weight of the TeLC mice was still lower than that of the GFP mice (8 weeks of HFD; Supplementary Fig. 4a). We found no significant differences in organ weight between TeLC and GFP mice (Supplementary Fig. 4b). However, histological analysis revealed a lower amount of lipid droplets in the brown adipose tissue (BAT; Fig. 6l) and liver (Fig. 6m) of the TeLC mice than in control mice. Consistently, the TeLC mice had less white adipose tissue (WAT) and BAT (Fig. 6n). The adipocyte size in iWAT and

epididymal WAT (eWAT) was correspondingly decreased in these mice (Fig. 6o,p). Furthermore, iWAT of some TeLC mice contained multilocular lipid droplets (Fig. 6o), suggesting lipid browning. In line with this observation, we found that the expression of *Ucp1* (the gene encoding uncoupling protein 1) was higher in the iWAT of TeLC mice than in control mice (Fig. 6q).

Together, these data show that inactivation of IPAC^{Nts} neurons efficiently protects from obesity and related detrimental health effects associated with an unhealthy diet by promoting metabolic changes favoring energy expenditure.

IPAC^{Nts} neurons form a network regulating energy homeostasis

We next sought to understand how IPAC^{Nts} neurons are connected to known feeding systems by mapping their afferent and efferent connections. To map the monosynaptic inputs to IPAC^{Nts} neurons, we injected a Cre-dependent monosynaptic retrograde rabies system in the IPAC of *Nts^{Cre}* mice (Fig. 7a,b and Methods). We found that IPAC^{Nts} neurons receive inputs (GFP⁺ cells) from several brain regions whose role in feeding and energy homeostasis has been well documented, such as the BNST, the nucleus accumbens, the paraventricular nucleus of the thalamus, the tuberal nucleus, the parasubthalamic nucleus and others (Fig. 7b–d). Interestingly, we found inputs from brain areas involved in the perception of taste, such as the insular cortex (Fig. 7d), and odors, such as the piriform and entorhinal cortices (Fig. 7c,d), which could potentially process food-related sensory information and drive consummatory behaviors.

To determine the downstream targets of neurotensin neurons in the anterior EA, we injected a GFP fluorescent reporter virus in the IPAC of *Nts^{Cre}* mice (Fig. 7e) and an mCherry AAV in the medial BNST

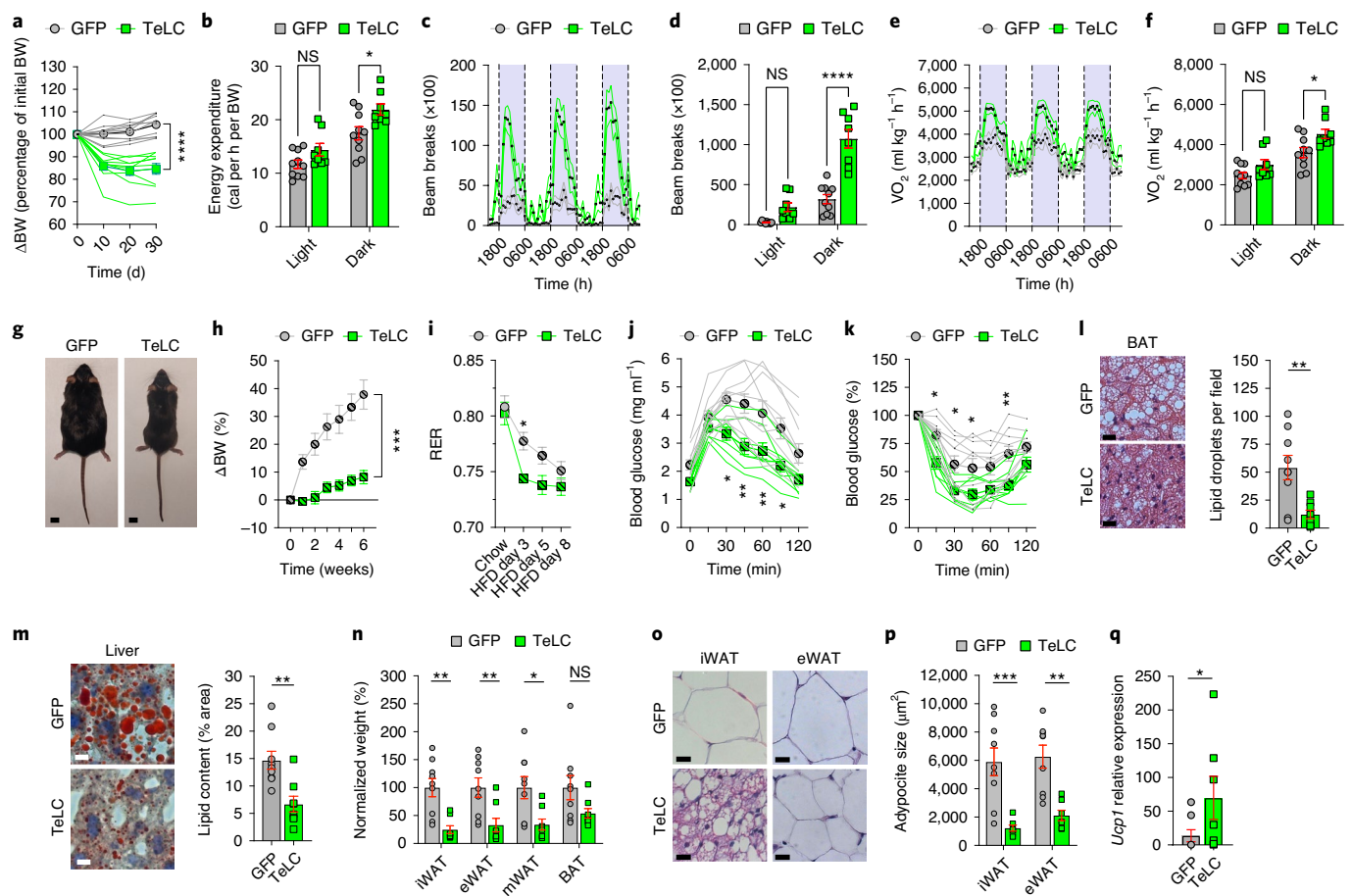


Fig. 6 | Inactivation of IPAC^{Nts} neurons protects from obesity and ameliorates metabolic syndrome. **a**, Body weight of GFP ($n = 11$) and TeLC ($n = 10$) mice fed chow; group effect: $F_{1,19} = 57.80$, $****P < 0.0001$. Data were analyzed by two-way RM ANOVA followed by a Sidak multiple comparisons test. **b**, Energy expenditure of GFP ($n = 10$) and TeLC mice ($n = 8$) fed chow; group effect: $F_{1,16} = 5.934$, $P = 0.0269$, $*P < 0.05$, $P > 0.05$ (NS). Data were analyzed by two-way RM ANOVA followed by a Sidak multiple comparisons test. **c, d**, Locomotor activity of GFP ($n = 10$) and TeLC ($n = 8$) mice fed chow. **c**, Interaction effect: $F_{70,1120} = 7.699$, $P < 0.0001$. Data were analyzed by two-way RM ANOVA. **d**, Group effect: $F_{1,16} = 37.84$, $P < 0.0001$, $****P < 0.0001$, $P > 0.05$ (NS). Data were analyzed by two-way RM ANOVA followed by a Sidak multiple comparisons test. **e, f**, Oxygen consumed (VO_2) by GFP ($n = 10$) and TeLC ($n = 8$) mice fed chow. **e**, Interaction effect: $F_{70,1120} = 2.221$, $P < 0.0001$. Data were analyzed by two-way RM ANOVA. **f**, Group effect: $F_{1,16} = 5.604$, $*P = 0.0309$, $P > 0.05$ (NS). Data were analyzed by two-way RM ANOVA followed by a Sidak multiple comparisons test. **g**, A representative GFP mouse and a TeLC mouse under a DIO paradigm; scale bar, 1 cm. **h**, Body weight of mice under a DIO paradigm; GFP ($n = 10$), TeLC ($n = 8$); group effect: $F_{1,16} = 19.72$, $****P < 0.0004$. Data were analyzed by two-way RM ANOVA. **i**, RER of mice under a DIO paradigm; GFP ($n = 10$), TeLC ($n = 8$); group effect: $P_{1,16} = 10.71$, $*P < 0.05$. Data were

analyzed by two-way RM ANOVA followed by a Sidak multiple comparisons test. **j, k**, Blood glucose levels during GTT (**j**) and ITT (**k**) of mice under a DIO paradigm; GFP ($n = 10$), TeLC ($n = 8$). **j**, Group effect: $F_{1,16} = 8.366$, $P = 0.0106$. **k**, Group effect: $F_{1,16} = 9.683$, $P = 0.0067$, $*P < 0.05$, $**P < 0.01$. Data were analyzed by two-way RM ANOVA followed by a Sidak multiple comparisons test. **l**, Left, BAT tissue of mice under a DIO paradigm (H&E staining); scale bar, 20 μm . Right, number of lipid droplets in BAT; GFP ($n = 9$) and TeLC ($n = 8$); $**P = 0.0037$. Data were analyzed by unpaired t -test. **m**, Left, liver tissue of mice under a DIO paradigm (red oil staining); scale bar, 10 μm ; right, area of lipid droplets in the liver; GFP ($n = 9$) and TeLC ($n = 8$); $**P = 0.0025$. Data were analyzed by unpaired t -test. **n**, WAT weight normalized to GFP mice; GFP ($n = 9$) and TeLC ($n = 8$); group effect: $F_{1,15} = 9.757$, $P = 0.0070$, $*P < 0.05$, $**P < 0.01$, $P > 0.05$ (NS). Data were analyzed by two-way RM ANOVA followed by a Sidak multiple comparisons test. mWAT, mesenteric WAT. **o**, WAT of mice under a DIO paradigm (H&E staining); scale bar, 20 μm . **p**, Adipocyte size; group effect: GFP ($n = 9$) and TeLC ($n = 7$), $F_{1,14} = 19.8$, $P = 0.0005$, $**P < 0.01$, $***P < 0.001$. Data were analyzed by two-way RM ANOVA followed by a Sidak multiple comparisons test. **q**, Expression of *Ucp1* in inguinal WAT (iWAT) of mice under a DIO paradigm; GFP ($n = 8$) and TeLC ($n = 7$); $*P = 0.0289$. Data were analyzed by Mann–Whitney U -test and are presented as mean \pm s.e.m.

(mBNST) of the same mice (Fig. 7e). We found that IPAC neurons project to a vast number of brain regions¹⁴. However, the projection pattern of the *Nts*⁺ neurons appears to be more restricted and includes the central EA (EAc; sometimes referred to as the sublenticular EA (SLEAc))¹⁴, the lateral hypothalamus (LHA), the substantia nigra pars compacta (SNc) and the retrorubral field (Fig. 7f). However, mBNST^{Nts} neurons have distinct projection targets or, if within the same downstream target area, clearly distinct spatial domains from IPAC^{Nts} neurons (Fig. 7f,g and Extended Data Fig. 6a).

The LHA is a highly heterogeneous area, regulating energy intake, energy expenditure, autonomic function, food preference and many other important physiological functions³⁰. We hypothesized

that activation of the IPAC^{Nts} \rightarrow LHA pathway could recapitulate the effects on feeding we observed when activating the IPAC^{Nts} somata. First, we performed monosynaptic retrograde tracing experiments by injecting the LHA with the cholera toxin B subunit (CT-B; Methods) and confirmed that IPAC^{Nts} neurons project to this location (Fig. 7h and Extended Data Fig. 6b). Next, we selectively activated these neurons in sated mice with optogenetics, similar to what we did for testing optogenetic manipulation of the IPAC^{Nts} somata (Fig. 7i,j, Extended Data Fig. 6c, Supplementary Fig. 5a and Methods). We found that photostimulation in Chr2 (but not GFP) mice significantly and preferentially increased energy intake on a HFD and WCh but not on chow or DCh (Fig. 7k). In addition, photostimulation produced

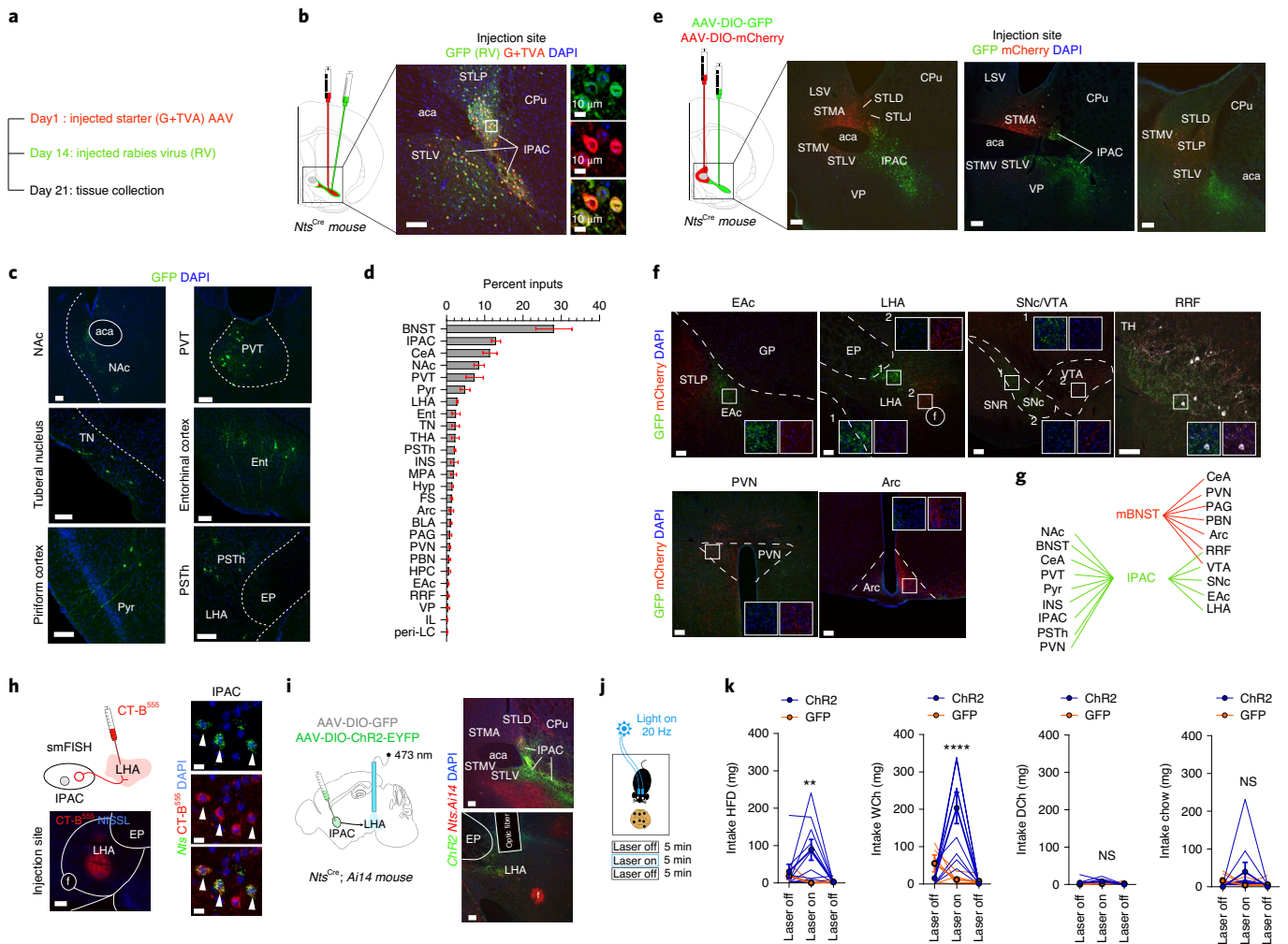


Fig. 7 | IPAC^{Nts} neurons send output and receive input to and from brain regions involved in energy homeostasis. **a**, Schematic of the strategy for monosynaptic retrograde rabies virus tracing. **b**, Representative image of the injection site; scale bar, 100 μ m. **c**, Representative images of the areas projecting to IPAC^{Nts} neurons; scale bar, 100 μ m. **d**, Brain regions projecting to IPAC^{Nts} neurons ($n = 3$). **e**, Representative images of the injection sites from a *Nts^{Cre}* mouse injected with multicolor Cre-dependent AAVs (GFP in the IPAC and mCherry in the mBNST); scale bar, 200 μ m. **f**, Representative images of brain areas innervated by IPAC^{Nts} (green) and mBNST^{Nts} (red) neurons; scale bar, 100 μ m. TH, tyrosine hydroxylase. **g**, Diagram illustrating brain regions upstream and downstream of IPAC^{Nts} neurons. **h**, Schematic of the retrograde strategy to label IPAC^{Nts} neurons projecting to the LHA (left, top) and representative images of the injection site (left, bottom; scale bar, 200 μ m) and of FISH for *Nts* on retrograde-labeled CT-B⁺ neurons in the IPAC (right; scale bar, 10 μ m). **i**, Left, schematic of the strategy to activate the IPAC^{Nts} \rightarrow LHA pathway; right, representative image showing Chr2 expression in IPAC^{Nts} neurons and an optical fiber tract on the LHA from a representative *Nts^{Cre}; Ai14* mouse; scale bar, 100 μ m. **j**, Schematic of the paradigm

for testing the effects of optogenetics on feeding behavior. **k**, Effect of light delivery into the LHA of mice injected in the IPAC with Chr2 or GFP and fed HFD, WCh, DCh or chow; Chr2 mice ($n = 9$) and GFP mice ($n = 5$); HFD, interaction effect: $F_{2,24} = 3.834, P = 0.0359$; WCh, interaction effect: $F_{2,24} = 13.19, P = 0.0001$; DCh, interaction effect: $F_{2,24} = 1.807, P = 0.1858$; chow, interaction effect: $F_{2,24} = 1.756, P = 0.1942$. Data were analyzed by two-way RM ANOVA followed by a Sidak multiple comparison test; ** $P < 0.01$, **** $P < 0.0001, P > 0.05$ (NS). Abbreviations: EP, endopenduncular nucleus; NAc, nucleus accumbens; GP, globus pallidus; SNR/C, substantia nigra, reticularis/compacta; TN, tuberal nucleus; Ent, entorhinal cortex; Pyr, piriform cortex; VTA, ventral tegmental area; RRF, retrorubral field; PVN, paraventricular nucleus; PVT, paraventricular thalamic nucleus; PSTh, parasubthalamic nucleus; CeA, central amygdala; Hyp, other hypothalamic nuclei; THA, other thalamic nuclei; PBN, parabrachial nucleus; INS, insular cortex; LC, locus coeruleus; BLA, basolateral amygdala; PAG, periaqueductal gray; TVA, receptor for the avian virus envelope protein EnvA; G, envelope glycoprotein; RV, rabies virus; MPA, medial preoptic area; HPC, hippocampus; EAc, extended amygdala cent; IL, infralimbic cortex; f, fornix.

intense gnawing but not consumption of inedible objects (that is, an eraser; Extended Data Fig. 6d), suggesting that the effect is food specific. Lastly, activation of this pathway is rewarding (Extended Data Fig. 6e).

Altogether, these data unveil the network of IPAC^{Nts} neurons and suggest that these neurons might control energy homeostasis by receiving inputs from feeding-relevant regions encoding taste- and odor-related sensory stimuli (for example, the piriform cortex) and projecting to the LHA to regulate feeding behavior and energy maintenance.

Discussion

Here, we show a role for IPAC^{Nts} neurons in encoding preference for ‘unhealthy’ foods and regulating dietary choices and energy behaviors. IPAC^{Nts} neurons are activated preferentially by palatable food and hedonic sensory stimuli (that is, taste and odor). Their response magnitude increases with hunger and stimulus palatability and strongly correlates with the mouse’s preference for the tastant. Of note, the preference for food encoded by IPAC^{Nts} neurons is dissociable from the nutritional value of the stimulus, suggesting an idiosyncratic and nuanced role in shaping dietary choices. Intriguingly, we show

that IPAC^{Nts} neurons are rapidly activated by sensory cues that anticipate food presence (for example, odors) and thus might act, similar to arcuate hypothalamic nucleus^{AgRP} (Arc^{AgRP}) cells, as 'feed-forward' neurons to guide food seeking and feeding^{31,32}. In line with this, we found that IPAC^{Nts} neurons receive strong input from cortical areas that detect and integrate taste (insular cortex) and smell cues (piriform and entorhinal cortex)^{12,33–35}.

Activation of IPAC^{Nts} neurons promotes intake of diets and liquids as a function of their palatability. However, we also show that activation of IPAC^{Nts} neurons is sufficient to modulate food palatability even once the initial preference is established. This suggests that the activity of IPAC^{Nts} neurons is important both for establishing dietary choices and guiding consumption. These effects are dissociable from the diet's nutritional value, suggesting that IPAC^{Nts} neurons encode orosensorial, rather than solely nutritional, reward stimuli. Importantly, our *Fos*, photometry and activation data suggest that IPAC^{Nts} neurons do not directly represent the specific motor actions of consumption.

Conversely, acute inhibition of IPAC^{Nts} neurons reduces feeding in hungry mice and reduces feeding on a HFD in sated mice, whereas it does not seem to affect homeostatic drinking or locomotor activity. These findings further suggest a specific role for IPAC^{Nts} neurons in regulating energy homeostasis. Chronic inhibition (that is, inactivation) of the activity of IPAC^{Nts} neurons demonstrates that the acute deficit on feeding observed with transient inhibition can be extended for days, reduce caloric intake and prevent weight gain.

We propose that the feeding deficit is mainly due to disrupted orosensorial perception. Photometry data show that IPAC^{Nts} neurons are rapidly activated when stimuli are presented. Furthermore, feeding deficits in acute inhibition experiments appear before postingestive effects are likely to take place (less than 30 min). In line with this, we show that inactivation of IPAC^{Nts} neurons impairs the mouse's ability to establish a preference for a tastant solely based on the perception of its hedonic value (that is, taste) over longer periods (that is, 72 h), whereas the ability of TeLC mice to form a preference for caloric compounds (eliciting postingestive effects) is intact. These results are consistent with previous findings suggesting that hedonic and homeostatic circuits are only partially overlapping⁸. For example, *Trpm5*-deficient mice are unable to sense sweet taste but are able to detect sucrose on the basis of its caloric content^{36,37}.

It is well established that a lack of physical activity is a major cause of the current obesity pandemic¹, and adherence to exercise routines is a first-line intervention for treating symptoms of obesity. We show that prolonged inactivation of IPAC^{Nts} neurons causes a dramatic increase in aerobic locomotion and long-term weight loss in non-obese mice. Although it might appear somewhat surprising that acute inhibition of IPAC^{Nts} neurons is not sufficient to elicit changes in energy expenditure, it is not unheard of that transient and chronic manipulation of the same neuronal ensembles can result in clearly different behavioral output³⁸. Along this line, the locomotor effects observed could be mediated by the neuropeptide neurotensin, whose kinetics are slower³⁹ than the neurotransmitter GABA. Of note, neurotensin receptor type 1 (*Ntsr1*) was reported to regulate energy expenditure and locomotor behavior in the SNc/ventral tegmental area complex⁴⁰, and we and others showed that neurotensin-expressing neurons in the IPAC project to this area⁴¹. Another possibility is that IPAC^{Nts} neurons are heterogeneous, such that some are involved in controlling hedonic eating and others are involved in regulating physical activities. TeLC inhibition would therefore affect both functions.

TeLC mice were preferentially active during their active phase (that is, the dark cycle), and GFP and TeLC mice had similar locomotion behaviors during anxiogenic tests, suggesting that the increase in physical activity in the TeLC mice is context or state dependent and may reflect volitional activities in a familiar environment.

Inactivation of IPAC^{Nts} neurons effectively protects mice from obesity and from the deleterious metabolic consequences of chronic feeding

on an unhealthy diet. These adaptations are likely the result of multiple metabolic changes. For instance, TeLC mice adapt more rapidly to a HFD than the less active control mice and exhibit enhanced lipid oxidation. Further, the fat deposits of TeLC mice dissipate energy by becoming metabolically active⁴². Both adaptations increase energy expenditure and likely contribute to the lean phenotype of the TeLC mice after prolonged exposure to an energy-dense diet. In addition, inactivation of IPAC^{Nts} neurons improves glucose metabolism and reduces lipid accumulation in BAT and liver tissues of the TeLC mice fed the HFD, suggesting a role in preventing BAT dysfunction (that is, BAT 'whitening')⁴³ and non-alcoholic fatty liver disease⁴⁴ associated with obesity in humans.

Finally, we provide a map of the brain areas upstream and downstream of IPAC^{Nts} neurons. Interestingly, IPAC^{Nts} neurons receive monosynaptic inputs from many brain areas implicated in feeding, energy balance and taste and odor perception. In line with previous studies, we found strong local connections within the IPAC and with the nearby BNST, to which the IPAC is intimately related. Other areas containing satiety-regulating neurons and projecting to IPAC^{Nts} neurons include the paraventricular nucleus and the Arc^{2,3}.

Neurotensin neurons in the anterior part of the EA area form a continuum between the IPAC, the FS and most lateral nuclei of the BNST. We show that IPAC^{Nts} neurons and *Nts*⁺ neurons in the medial nuclei of the BNST (mBNST^{Nts} neurons) are part of distinct networks. IPAC^{Nts} neurons project to the EAc (sometimes referred to as the SLEAc)¹⁴, the SNc and the most lateral part of the LHA. Interestingly, activation of the IPAC^{Nts} → LHA pathway induces feeding on energy-dense foods and is rewarding, thus partially recapitulating the behaviors deriving from somata activation. This projection pattern suggests that IPAC^{Nts} neurons might belong to the medial, rather than the lateral, division of the IPAC¹⁴, which was reported to be intimately associated with the BNST and the EA¹⁴. Considering the profound degree of interconnection with EA territories, we propose that *Nts*-expressing neurons in the IPAC could label a previously unnoticed more lateral nucleus of the BNST. More experiments are needed to address whether mBNST^{Nts} neurons projecting to the LHA and other regions have similar or distinct roles on feeding and energy homeostasis.

Altogether, our data suggest that the *Nts* gene is a useful marker to genetically access this previously uncharacterized brain area. IPAC^{Nts} neurons appear to be homogeneous regarding their activity; aversive odors (that is, BA) do not activate IPAC^{Nts} neurons, suggesting the absence of subpopulations encoding aversive stimuli, as reported by studies investigating the role in learned disgust^{10,11} in more posterior IPAC territories. In line with this, IPAC^{Nts} neurons are intrinsically rewarding, and their projection pattern is clearly distinct from other *Nts*⁺ populations. Nonetheless, because our investigation has been performed at the population level, it is possible that a more in-depth characterization of this area might reveal currently unappreciated molecular heterogeneity of its neurons.

In conclusion, we identified a single, extrahypothalamic population of neurons with crucial roles in promoting metabolic responses via behavior modification. From a therapeutic point of view, these findings are highly relevant as they show that blocking a handful of molecularly defined neurons (1) leads to long-term weight loss, (2) has beneficial effects on metabolic function and (3) protects from obesity and metabolic syndromes. Conceptually, this brain area is an ideal entry point to unravel the complex brain–metabolism regulatory loop underlying body weight homeostasis.

Online content

Any methods, additional references, Nature Research reporting summaries, source data, extended data, supplementary information, acknowledgements, peer review information; details of author contributions and competing interests; and statements of data and code availability are available at <https://doi.org/10.1038/s41593-022-01178-3>.

References

1. Bluher, M. Obesity: global epidemiology and pathogenesis. *Nat. Rev. Endocrinol.* **15**, 288–298 (2019).
2. Fenselau, H. et al. A rapidly acting glutamatergic ARC→PVH satiety circuit postsynaptically regulated by α -MSH. *Nat. Neurosci.* **20**, 42–51 (2017).
3. Li, M. M. et al. The paraventricular hypothalamus regulates satiety and prevents obesity via two genetically distinct circuits. *Neuron* **102**, 653–667 (2019).
4. Zhang, X. & van den Pol, A. N. Rapid binge-like eating and body weight gain driven by zona incerta GABA neuron activation. *Science* **356**, 853–859 (2017).
5. Speakman, J. R. et al. Set points, settling points and some alternative models: theoretical options to understand how genes and environments combine to regulate body adiposity. *Dis. Model Mech.* **4**, 733–745 (2011).
6. Trexler, E. T., Smith-Ryan, A. E. & Norton, L. E. Metabolic adaptation to weight loss: implications for the athlete. *J. Int Soc. Sports Nutr.* **11**, 7 (2014).
7. Hill, J. O., Wyatt, H. R. & Peters, J. C. Energy balance and obesity. *Circulation* **126**, 126–132 (2012).
8. Rossi, M. A. & Stuber, G. D. Overlapping brain circuits for homeostatic and hedonic feeding. *Cell Metab.* **27**, 42–56 (2018).
9. Alheid, G. F. Extended amygdala and basal forebrain. *Ann. N. Y. Acad. Sci.* **985**, 185–205 (2003).
10. Tanaka, D. H., Li, S., Mukae, S. & Tanabe, T. Genetic access to gustatory disgust-associated neurons in the interstitial nucleus of the posterior limb of the anterior commissure in male mice. *Neuroscience* **413**, 45–63 (2019).
11. Tanaka, D. H., Li, S., Mukae, S. & Tanabe, T. Genetic recombination in disgust-associated bitter taste-responsive neurons of the central nucleus of amygdala in male mice. *Neurosci. Lett.* **742**, 135456 (2021).
12. Gehrlach, D. A. et al. A whole-brain connectivity map of mouse insular cortex. *eLife* **9**, e55585 (2020).
13. Madisen, L. et al. A robust and high-throughput Cre reporting and characterization system for the whole mouse brain. *Nat. Neurosci.* **13**, 133–140 (2010).
14. Shammah-Lagnado, S. J., Alheid, G. F. & Heimer, L. Striatal and central extended amygdala parts of the interstitial nucleus of the posterior limb of the anterior commissure: evidence from tract-tracing techniques in the rat. *J. Comp. Neurol.* **439**, 104–126 (2001).
15. Steculorum, S. M. et al. AgRP neurons control systemic insulin sensitivity via myostatin expression in brown adipose tissue. *Cell* **165**, 125–138 (2016).
16. Atasoy, D., Betley, J. N., Su, H. H. & Sternson, S. M. Deconstruction of a neural circuit for hunger. *Nature* **488**, 172–177 (2012).
17. Chen, T. W. et al. Ultrasensitive fluorescent proteins for imaging neuronal activity. *Nature* **499**, 295–300 (2013).
18. O'Connor, E. C. et al. Accumbal D1R neurons projecting to lateral hypothalamus authorize feeding. *Neuron* **88**, 553–564 (2015).
19. Tan, H. E. et al. The gut–brain axis mediates sugar preference. *Nature* **580**, 511–516 (2020).
20. Yeomans, M. R. Taste, palatability and the control of appetite. *Proc. Nutr. Soc.* **57**, 609–615 (1998).
21. Patel, J. M. et al. Sensory perception drives food avoidance through excitatory basal forebrain circuits. *eLife* **8**, e44548 (2019).
22. Riera, C. E. et al. The sense of smell impacts metabolic health and obesity. *Cell Metab.* **26**, 198–211 (2017).
23. Cabanac, M. Physiological role of pleasure. *Science* **173**, 1103–1107 (1971).
24. Jennings, J. H., Rizzi, G., Stamatakis, A. M., Ung, R. L. & Stuber, G. D. The inhibitory circuit architecture of the lateral hypothalamus orchestrates feeding. *Science* **341**, 1517–1521 (2013).
25. Vardy, E. et al. A new DREADD facilitates the multiplexed chemogenetic interrogation of behavior. *Neuron* **86**, 936–946 (2015).
26. Murray, A. J. et al. Parvalbumin-positive CA1 interneurons are required for spatial working but not for reference memory. *Nat. Neurosci.* **14**, 297–299 (2011).
27. Strelakova, T., Spanagel, R., Dolgov, O. & Bartsch, D. Stress-induced hyperlocomotion as a confounding factor in anxiety and depression models in mice. *Behav. Pharmacol.* **16**, 171–180 (2005).
28. Trajceviski, K. E. et al. Enhanced lipid oxidation and maintenance of muscle insulin sensitivity despite glucose intolerance in a diet-induced obesity mouse model. *PLoS ONE* **8**, e71747 (2013).
29. O'Neal, T. J., Friend, D. M., Guo, J., Hall, K. D. & Kravitz, A. V. Increases in physical activity result in diminishing increments in daily energy expenditure in mice. *Curr. Biol.* **27**, 423–430 (2017).
30. Berthoud, H. R. & Munzberg, H. The lateral hypothalamus as integrator of metabolic and environmental needs: from electrical self-stimulation to opto-genetics. *Physiol. Behav.* **104**, 29–39 (2011).
31. Chen, Y., Lin, Y. C., Kuo, T. W. & Knight, Z. A. Sensory detection of food rapidly modulates arcuate feeding circuits. *Cell* **160**, 829–841 (2015).
32. Lowell, B. B. New neuroscience of homeostasis and drives for food, water, and salt. *N. Engl. J. Med.* **380**, 459–471 (2019).
33. Terral, G. et al. CB1 receptors in the anterior piriform cortex control odor preference memory. *Curr. Biol.* **29**, 2455–2464 (2019).
34. Xu, W. & Wilson, D. A. Odor-evoked activity in the mouse lateral entorhinal cortex. *Neuroscience* **223**, 12–20 (2012).
35. Bitzenhofer, S. H., Westeinde, E. A., Zhang, H. B. & Isaacson, J. S. Rapid odor processing by layer 2 subcircuits in lateral entorhinal cortex. *eLife* **11**, e75065 (2022).
36. de Araujo, I. E. et al. Food reward in the absence of taste receptor signaling. *Neuron* **57**, 930–941 (2008).
37. Beeler, J. A. et al. Taste uncoupled from nutrition fails to sustain the reinforcing properties of food. *Eur. J. Neurosci.* **36**, 2533–2546 (2012).
38. Urban, D. J. et al. Elucidation of the behavioral program and neuronal network encoded by dorsal raphe serotonergic neurons. *Neuropsychopharmacology* **41**, 1404–1415 (2016).
39. Blaha, C. D. & Phillips, A. G. Pharmacological evidence for common mechanisms underlying the effects of neurotensin and neuroleptics on in vivo dopamine efflux in the rat nucleus accumbens. *Neuroscience* **49**, 867–877 (1992).
40. Woodworth, H. L. et al. Neurotensin receptor-1 identifies a subset of ventral tegmental dopamine neurons that coordinates energy balance. *Cell Rep.* **20**, 1881–1892 (2017).
41. Woodworth, H. L., Brown, J. A., Batchelor, H. M., Bugescu, R. & Leininger, G. M. Determination of neurotensin projections to the ventral tegmental area in mice. *Neuropeptides* **68**, 57–74 (2018).
42. Aldiss, P. et al. Exercise-induced 'browning' of adipose tissues. *Metabolism* **81**, 63–70 (2018).
43. Shimizu, I. et al. Vascular rarefaction mediates whitening of brown fat in obesity. *J. Clin. Invest.* **124**, 2099–2112 (2014).
44. Recena Aydos, L. et al. Nonalcoholic fatty liver disease induced by high-fat diet in C57BL/6 models. *Nutrients* **11**, 3067 (2019).

Publisher's note Springer Nature remains neutral with regard to jurisdictional claims in published maps and institutional affiliations.

Springer Nature or its licensor (e.g. a society or other partner) holds exclusive rights to this article under a publishing agreement with the author(s) or other rightsholder(s); author self-archiving of the accepted manuscript version of this article is solely governed by the terms of such publishing agreement and applicable law.

© The Author(s), under exclusive licence to Springer Nature America, Inc. 2022

Methods

Animals

Male and female mice of at least 2 months of age were used for all experiments. Mice were housed in their home cages (two to five mice per cage) under a 12-h light/12-h dark cycle, with food and water freely available. Ambient temperature (21–22 °C) and humidity (62%) were automatically controlled. All behavioral experiments were performed during the light cycle. All experimental procedures were approved by the Institutional Animal Care and Use Committee of Cold Spring Harbor Laboratory and performed in accordance with the US National Institutes of Health guidelines in an AAALACi-accredited facility. The *Nts^{Cre}* mouse line (stock number 017525) and *Ail4* (stock number 007908) and wild-type mice (stock number 000664) were purchased from Jackson Laboratories and bred onto a C57BL/6J background.

Viral vectors

- AAV9-pCAG-Flex-EGFP-WPRE (Addgene, 51502)
- AAV5-pAAV-hSyn-DIO-EGFP (Addgene, 50457)
- AAV9-EF1a-DIO-hChr2(H134R)-eYFP-WPRE-hGH (Addgene, 20298)
- AAV2/9-CAG-DIO-TeLC-eGFP, previously described in ref. 26.
- AAV1-Syn.Flex.GCaMP6f.WPRE.SV40 (Addgene, 100833)
- AAV8-pAAV-hSyn-df-HA-KORD-IRES-mcritrine (Addgene, 65417)
- AAV2-pAAV-hSyn-DIO-mCherry (Addgene, 50459)
- rAAV-nEfla-DIO-NLS-mCherry-F2A-TVA-RVG.WPRE (Brain VTA, PT-0027)
- RV-ENVA-ΔG-EGFP (Brain VTA, R01001)

All viral vectors were aliquoted and stored at –80 °C until use.

Stereotaxic surgery

All surgery was performed under aseptic conditions. Mice were placed on a heating pad for the duration of the surgery. Surgical procedures were previously described^{45,46}. Briefly, after mice were anesthetized (1–2% isoflurane with oxygen applied at 1.0 liter min⁻¹), they were head fixed in the stereotaxic injection apparatus. Targeting of brain areas was done using a digital mouse brain atlas (Angle Two Stereotaxic System). Metacam (2 mg per kg (body weight)) was injected intraperitoneally (i.p.) as analgesic.

Once the mouse skull was exposed, we drilled a cranial window (1–2 mm²) unilaterally (in vivo photometry, monosynaptic rabies and anterograde tracing experiments) or bilaterally (optogenetic and chemogenetic experiments). Next, a glass capillary was lowered into the window to deliver ~0.1 μl of viral vector to the area of interest (coordinates: IPAC 0.40 mm anterior to bregma, 1.45 mm lateral from midline and –4.50 mm vertical from the brain surface; BNST: 0.00 mm anterior to bregma, 0.90 mm lateral from midline and –4.20 mm vertical from the brain surface). The viral solution was delivered at a rate of ~20 nl min⁻¹ using a Picospritzer III (General Valve) and a pulse generator (Agilent) generating pressure bursts (5–20 psi, 5–20 ms at 1 Hz). Following delivery, the pipette was left in place for 10 min and carefully withdrawn.

For mice for in vivo photometry and optogenetics experiments, following viral delivery, we implanted optic fibers above injection locations (coordinates: IPAC: 0.40 mm anterior to bregma, 1.45 mm lateral from midline and 4.30 mm vertical from the brain surface; LHA: 1.40 mm posterior to bregma, 1.15 mm lateral from midline and 5.00 mm vertical from the brain surface). When needed, a head bar was also mounted to facilitate head restraint. *Nts^{Cre}* mice used for rabies tracing were first unilaterally injected in the IPAC with the starter AAV. After 14 d, the same mice were injected with the rabies virus. Seven days later, mice were killed, and their brain tissue was collected and processed for immunohistochemistry. *Nts^{Cre}* mice used for anterograde experiments were injected unilaterally in the IPAC and BNST. After 3 weeks, mice were killed, and their brain tissue was collected and processed for immunohistochemistry. A cohort of wild-type mice

was unilaterally injected in the LHA with Alexa⁵⁵⁵-conjugated CT-B (Invitrogen, Thermo Fisher Scientific; 0.2 μl, 1 mg ml⁻¹ in PBS). Mice were perfused 5 d after the injection. Brain tissue was collected and processed for smFISH.

In vivo fiber photometry experiments in freely moving mice

To record the activity of IPAC^{Nts} neurons in behaving animals, we used a commercial fiber photometry system (Neurophotometrics) and Bonsai software (v. 2.3.1) to measure GCaMP6f signals through an optical fiber unilaterally implanted above the IPAC (diameter: 200 μm; length: 5.0 mm; NA: 0.37; Inper). Mice were tethered to a patch cord (diameter: 200 μm; Doric Lenses) connected to the photometry system. The intensity of the LED light (λ = 470 nm) for excitation was adjusted to ~20 μW at the tip of the patch cord. Photometry signals and relevant behavioral events were aligned based on an analog TTL signal, and timing data were generated by a Bpod State machine (Sanworks).

To correct photobleaching of fluorescence signals, we fit a two-term exponential curve to the data to model photobleaching using the MathWorks fit function. We then used this fitted curve for ΔF/F₀ normalization, where ΔF is the change in fluorescence, and F₀ is baseline fluorescence, treating the fitted curve as baseline fluorescence in our calculation ΔF/F₀ = (F(t) – F₀(t))/F₀(t), where F is the raw fluorescence data and F₀ is the fitted curve. This gave us a corrected ΔF/F₀ that takes into account the slowly decreasing baseline. All photometry trials were randomly interspersed, so the differences seen in liquid responses were not due to bleaching or to our bleaching correction. The z score of ΔF/F₀ was then calculated using the mean and standard deviation of the signal during the baseline periods (the pooled 10-s time windows before each stimulus), z score (ΔF/F₀) = (ΔF/F₀ – mean (baseline ΔF/F₀))/standard deviation (baseline ΔF/F₀).

A small number of trials had artifacts due to coiling of the photometry fibers or movement of the animals. To find these trials, we automatically flagged for review any trial with a fluctuation of greater than three times the standard deviation of signal in the control channel. We discarded trials with substantial artifacts during the stimulus period. This method minimized the effect of movement artifacts on the signal.

Free-feeding tests. Mice were food restricted starting at 1700 h the day before the testing day. FR mice were presented with either a grain-based pellet (similar to the regular chow; 45 mg per pellet, Bioserv, F0165, 3.43 cal g⁻¹) or a lard-based high-fat pellet (Envigo custom diet, 4.5 cal g⁻¹) on consecutive days. Food presentation was randomized. After food restriction experiments, the same mice were given food and water ad libitum before being tested in sated conditions 48 h later with a lard-based high-fat pellet (Envigo custom diet, 4.5 cal g⁻¹). All feeding bouts lasted for at least 10 s.

Free drinking tests. Mice were water restricted starting at 1700 h the day before the training day. On the training day, mice learned to acquire water by licking at two adjacent spouts, with each spout delivering equal volumes of water in a random order. The spout also served as part of a custom ‘lickometer’ circuit, which registered a lick event each time a mouse completed the circuit by licking the spout. The training protocol required the mice to lick the spout with a water droplet before moving onto the next trial. Custom software written in MATLAB (MathWorks, R2017a) was used to control the delivery of liquids and record licking events through a Bpod State machine (Sanworks). Training consisted of one session of 100 trials. The next day, which was the testing day, the mice were tested with two pairs of liquids. Each pair of liquids was available in interleaved trials (25 trials for each pair, 50 trials in total; intertrial intervals, random between 8 and 14 s), and each liquid was delivered from one of the two spouts in equal volume. As the protocol required mice to lick the spouts to progress, we ensured that all of the liquids were consumed. The tubing and spouts were carefully washed between delivery of

different liquids. Volume calibration was performed before every test. In Fig. 2j, behavioral preference (preference) and the associated z score were calculated with the following equations:

$$z \text{ score } (\%) = \frac{z \text{ score (AUC) tastant A} - z \text{ score (AUC) tastant B}}{z \text{ score (AUC) tastant A} + z \text{ score (AUC) tastant B}}$$

$$\text{Preference } (\%) = \frac{\text{Licks per s tastant A} - \text{Licks per s tastant B}}{\text{Licks per s tastant A} + \text{Licks per s tastant B}}$$

In vivo fiber photometry experiments in head-fixed mice

For photometry experiments with the olfactometer, we used a custom-made fiber photometry system to measure GCaMP6f signals in vivo. Green- and red-emitted fluorescent signals were filtered and split to separate photodetectors and digitally sampled at 6,100 Hz via a data acquisition board (National Instruments, model NI USB-6211). Peaks were extracted by custom MATLAB software with an effective sampling rate of 211 Hz. Signals from each fiber were corrected for photobleaching by fitting the decay with a double exponential and then normalizing to a z score. The red signals represent autofluorescence and were used to monitor and correct for potential movement artifacts. The signals in the green channel were transformed back to absolute fluorescence, and $\Delta F/F$ was computed. The resulting traces from each recording session were converted to a z score to compare between mice. All data analysis was performed using custom-written code in MATLAB.

Mice were under head restraint in front of the output of a custom-built olfactometer. Before the testing, mice were habituated to the setup for 1 h. The odors were presented using the olfactometer, which contains an eight-way solenoid that controls oxygen flow through eight vials. The vials contained odorants dissolved in MO. The odors presented were BA (Sigma, 103500; 100 μ l dissolved in 5 ml of MO), OO-based HFD (Envigo; 1 g in 5 ml of MO), CO-based HFD (Envigo; 1 g in 5 ml of MO), WCh (Lindt; 1 g in 5 ml of MO), DCh (Ghirardelli; 1 g in 5 ml of MO), regular chow (PicoLab rodent diet 20, 5053*; 1 g in 5 ml of MO) and MO as a control (Sigma, M3516). Food pellets were crumbled and homogenized in MO for 10 min using a vortex mixer. Odorized oxygen was diluted 10:1 into a continuous carrier stream for a total flow of 4 liters min^{-1} . To prevent odor accumulation, air was collected behind the animal with a vacuum pump. Odor presentations were 3 s every 30 s while constantly measuring calcium signals in IPAC^{NIS} neurons. Every testing session consisted of 10 trials per odor. Mice in Fig. 3e were familiarized to the CO- and OO-based lard diets for 2 consecutive days, and preference was tested on the third day and based on their 3-h intake (see Food preference tests). Data in Fig. 3f–j were acquired from mice in Fig. 3e.

Behavioral assays

Optogenetic experiments. Feeding experiments. Mice sated on regular chow and HydroGel were tethered to the optic fiber patch cable and habituated to the behavior box for 10 min on the day before testing. On the testing day, following an additional habituation of 5 min, a food pellet or a liquid (in a metal cup) was placed on the floor of the box. Feeding behavior was assessed for 5 min with the laser off (baseline measure), then 5 min with the light on (20 Hz, 7–10 mW measured at the tip of the fiber) and then another 5 min with the laser off. The food was weighed before and after each of the 5-min sessions. Foods in Figs. 4b,c and 7k and Extended Data Figs. 3b,c,f and 6d were delivered on consecutive days in a randomized order; foods in Fig. 4g,h were presented within the same session (see Food preference tests). The foods used were grain-based pellets (similar to the regular chow; 45 mg per pellet, Bioserv, F0165, 3.43 cal g^{-1}), sucrose (45 mg per pellet, Bioserv, F0021, 3.83 cal g^{-1}), HFD (Bioserv, S3282, 5.49 cal g^{-1}), WCh (Lindt, 5.5 cal g^{-1}),

DCh (Ghirardelli, 5.5 cal g^{-1}), HFD^{CO} (Envigo custom diet, 4.5 cal g^{-1}) and HFD^{OO} (Envigo custom diet, 4.5 cal g^{-1}). An eraser from the tip of a pencil was used as inedible object. ‘Gnawing’ was quantified by subtracting the eraser weight after every session from the eraser weight at the beginning of the session. Plain and quinine-flavored grain-based pellets were prepared by immersing the pellets in either water or a 10 mM quinine solution for 10 min. Pellets were dried O/N and used for testing the following day.

To score feeding bouts, videos generated from the feeding behavioral assays were analyzed frame by frame using Behavioral Observation Research Interactive Software (BORIS v 7.12.2)⁴⁷. A feeding bout was defined as an event lasting for at least 3 s from pellet pickup to either pellet drop or pellet fully consumed.

Drinking experiments. The following liquids were presented: 30% sucrose in water (wt/vol), 10% sucrose in water (wt/vol), 0.1% sucralose in water (wt/vol), 5% fat emulsion (Intralipid), NaCl 75 mM in water (wt/vol), 10 mM citric acid in water, 1 mM quinine in water and water. Drinking behavior was assessed for 5 min with the laser off (baseline measure), 5 min with the light on (20 Hz, 7–10 mW measured at the tip of the fiber) and then another 5 min with the laser off. The liquids were weighed before and after each of the 5-min sessions. Liquids were presented on consecutive days to sated mice in a randomized order.

Conditioned flavor preference. Single-housed mice sated on chow were familiarized to the CO- and OO-based lard diets in 2 consecutive days. The baseline flavor preference was assessed by presenting mice with the two diets at the same time. Food preference was determined based on their 3-h intake over the second of 2 consecutive test days. Conditioning was performed for 4 d, with two sessions per day. Before each session, mice were tethered to the optic fiber patch cable and habituated to the behavioral chamber for 10 min. Conditioning consisted of pairing intracranial light pulses (473 nm, 8–10 mW, 30 Hz) with the less preferred diet (session 1). Four hours later, the same mice were presented with the more preferred diet without photostimulation (session 2). The order of the sessions was inverted every day. Photostimulation was delivered right after the mouse would spontaneously initiate food intake and lasted for as long as the pellet was consumed (each was 0.5 g). The investigator manually delivered the light pulses. Conditioned flavor preference was tested for 2 consecutive days after conditioning (day 5 and day 6). The preference of these two sessions was averaged.

Chemogenetic experiments. For chemogenetic experiments, experimental KORD and control mCherry mice were given a subcutaneous injection of SalB (10 mg per kg (body weight) in DMSO) or control vehicle (DMSO, volume equivalent). After the injection, mice were placed back in their home cages for 20 min before starting testing. The order of testing, on different days, was (1) FR mice had access to chow for 1 h, (2) mice sated (on chow) had access to a lard-based HFD (Envigo) for 1 h, (3) mice sated (on chow) were tested on locomotion assays and (4) WR mice had access to water for 1 h. For locomotor assays, mice were first introduced to a new semitransparent normal-sized cage for habituation. The arena was enclosed in a sound-attenuating chamber with a house light on the ceiling. After 30 min, mice were injected as described above and reintroduced into the cage, and their behavior (total distance traveled) was recorded for 60 min. Data were analyzed using the image processing and tracking software Ethovision XT 5.1 (Noldus Information Technologies).

Liquid preference tests. To test the preferences of sated mice between a sucralose solution (0.004%) and water or between a sucrose solution (1%) and water (Extended Data Fig. 4e), sated mice were singly housed with food and water available ad libitum for 1 week before the start of the experiment. Water was dispensed through a bottle in the cage. A second bottle containing either sucralose or sucrose solution was then added to the cage. Mice were allowed to first habituate to the newly

added solution for 24 h, after which their consumption of the solution and water over a 48-h period was measured. The testing of sucralose and sucrose was separated by a 48-h period, during which the mice had access only to water. The positions of the bottles were switched every 24 h to minimize a potential positional effect. Preference was calculated as

$$\text{Preference for A (\%)} = \frac{(\text{Intake liquid A})}{(\text{Intake liquid A} + \text{Intake liquid B})}$$

Food preference tests. Mice in Figs. 3e and 4g–j were familiarized with HFD^{CO} and HFD^{OO} for 2 d, during which HFD^{CO} or HFD^{OO} (0.5 g per mouse) was introduced in the home cage on consecutive days, with chow and water available ad libitum. Mice were singly housed. On test days, both HFD^{CO} and HFD^{OO} diets were presented simultaneously in the home cage, and intake was measured at 3 h after the delivery. Preference was calculated as

$$\text{Preference for CO (\%)} = \frac{(\text{Intake HFD}^{\text{CO}})}{(\text{Intake HFD}^{\text{CO}} + \text{Intake HFD}^{\text{OO}})}$$

Real-time place preference test. Mice sated on regular chow and HydroGel were tethered to an optic fiber patch cable. Mice were introduced to a 23 × 33 × 25 cm non-transparent, two-sided Plexiglas chamber, and their baseline preference for either side (left or right) was assessed for 10 min. Mice were tested across two sessions. In session one, one side was assigned as the photostimulation chamber. Every time the mouse would enter this chamber, 5-ms pulses at 30 Hz and 7–10 mW (measured at the tip of optic fibers) of blue light (473-nm laser (OEM Laser Systems)) were delivered intracranially. Photostimulation ceased when the mouse left the photostimulation side. In the second session, we assigned the other chamber as the photostimulation side and repeated testing. The behavior of the mice was videotaped with a camera. Ethovision software (Noldus Information Technologies) was used to deliver laser pulses and analyze behavioral parameters.

Intracranial self-stimulation tests. Mice sated on regular chow and HydroGel were tethered to an optic fiber patch cable and placed in a non-transparent, custom-made behavioral box equipped with two ports, one ‘active’ and one ‘inactive’. Poking into the active port would deliver light into the IPAC or the LHA (5-ms pulses, 20 Hz, 10 mW; $\lambda = 473$ nm), whereas poking into the inactive port would not. Mice were tested in this setup for up to 1 h.

For testing the impact of nutritional state on self-stimulation behavior, Chr2 mice were trained for two consecutive days for 1 h per day to nose poke to self-stimulate (delivering light into the IPAC) while sated on regular chow (PicoLab rodent diet 20, 5053*). Each nose poke produced a 2-s train of stimulation (5-ms pulses, 20 Hz, 10 mW; $\lambda = 473$ nm). Mice were then tested on consecutive days when fed regular chow, a HFD for 2 h before the test (HFD; Bioserv, S3282; physiological value, 5.49 kcal g⁻¹) or after being food restricted O/N.

OF locomotion test. OF tests for Chr2 mice were performed in a non-transparent square box of 42 × 21 × 15 cm. The arena was enclosed in a sound-attenuating chamber with a house light on the ceiling. Animals were placed in one of the corners of the OF arena at the start of a session. Locomotor behavior was assessed for 10 min with the laser off (baseline measure), 10 min with the light on (30 Hz, 7–10 mW measured at the tip of the fiber) and then another 10 min with the laser off. Behavior was videotaped, and the resulting data were analyzed using the image processing and tracking software Ethovision XT 5.1 (Noldus Information Technologies).

OF anxiety test. The OF test was performed in a non-transparent square box of 42.5 × 42.5 × 40 cm. This OF arena was enclosed in a

sound-attenuating chamber with a house light on the ceiling. At the start of the 10-min session, animals were placed in one of the corners of the arena and left free to explore. A light source was held above the OF box and projected intense bright light over a 21 × 21 cm square zone in the middle of the arena. Behavior was videotaped, and the resulting data were analyzed using the image processing and tracking software Ethovision XT 5.1 (Noldus Information Technologies).

EPM test. The EPM test consisted of a non-transparent, cross-shaped apparatus made of Plexiglass, two ‘closed’ arms enclosed by 15-cm-high walls and two ‘open’ arms without walls. The arms were 30 cm long and 5 cm wide and extended from a central platform (5 × 5 cm) to allow mice to freely move across the arms of the setup. The maze was elevated at a height of 55 cm from the ground. At the start of the 10-min sessions, mice were placed in the central zone. Behavior was videotaped, and the resulting data were analyzed using the image processing and tracking software Ethovision XT 5.1 (Noldus Information Technologies).

Physiological assays

Metabolic cages. Mice were singly housed and habituated to the metabolic cages (CLAMS, Columbus) for at least 1 week before testing under a 12-h light/12-h dark cycle. Mice used in the control and experimental groups (that is, GFP and TeLC mice) were age matched. Locomotor activity (infrared beam breaks in the xyz axis), energy expenditure, VO₂, VCO₂, RER, food intake and water intake were recorded. Data were exported using Clax software v2.2.0 and were analyzed in Excel (2019). For 72-h visualizations, data were binned in 1-h intervals. White and purple represent light (0600–1800) and dark (1800–0600) cycles, respectively. Heat (renamed energy expenditure), VO₂ and VCO₂ data were normalized to body weight. The mice were first fed with regular chow (PicoLab rodent diet 20, 5053*; physiological value, 3.43 kcal g⁻¹) and then with a HFD (Bioserv, S3282; physiological value, 5.49 kcal g⁻¹). Diets and water were freely available during testing. Gas sensor calibration (CO₂ and O₂) of the apparatus was performed before each test. Mouse body weight was recorded before and after every testing session.

ITT and GTT. Singly housed mice were transferred to a clean cage with food removed for 6 h (0900–1500) before each test. All tests started at 1500 h. For the ITT, mice were injected i.p. with 0.5 U per kg (body weight) insulin (Humulin, Eli Lilly; NDC code 0002–8215) in 0.9% sterile saline. For the GTT, mice were injected i.p. with 1 g per kg (body weight) glucose (Sigma, G5767-25G) in 0.9% sterile saline. There was a 48-h gap between tests, during which food and water were available ad libitum. Blood glucose levels were measured in duplicate after injection using the OneTouch Ultra 2 Glucometer (OneTouch).

Immunohistochemistry

Immunohistochemistry protocols were previously described⁴⁵. Briefly, mice were deeply anesthetized and perfused with 50 ml of PBS, followed by 50 ml of 4% paraformaldehyde (PFA) in PBS. The extracted brains were kept in 4% PFA O/N and the following day were transferred to a 30% sucrose solution (in PBS) at 4 °C. After 48 h, brain tissue was cut on a microtome (Leica, SM2010R). The 50- μ m coronal brain sections were incubated with the appropriate primary antibodies diluted in a PBS solution containing 1% Tween-20 (PBS-T; Sigma, P2287) O/N at 4 °C. The following day, the sections were washed in PBS-T twice and incubated with secondary antibody diluted in PBS-T for 2 h at room temperature. Sections were then washed in PBS-T twice and incubated with DAPI (Invitrogen, D1306; 0.5 μ g ml⁻¹ in PBS) for 5 min, washed twice again in PBS-T and mounted onto slides with Fluoromount-G (eBioscience). Images were taken using an LSM710 or LSM780 confocal microscope (Carl Zeiss) and visualized and processed using ImageJ (1.53q) and Adobe Illustrator (CS6, version 16.0.0).

The primary antibodies used were chicken anti-GFP (1:1,000; Aves Labs, GFP1020), rabbit anti-RFP (1:1,000; Rockland, 600-401-379,

35868), rabbit anti-HA-tag (1:1,000; Cell Signaling, 3724S), rabbit anti-mCherry (1:1,000; Abcam, ab167453, GR3213077-3), rabbit anti-TH (1:1,000, Millipore, AB152) and goat anti-AgRP (1:200; R&D, AF634). The secondary antibodies used were Alexa Fluor 488 donkey anti-chicken (1:1,000; Jackson ImmunoResearch, 703-545-155), Alexa Fluor 647 donkey anti-chicken (1:1,000; Jackson ImmunoResearch, 703-606-155), Alexa Fluor 647 donkey anti-goat IgG (1:1,000; Jackson ImmunoResearch, 703-605-003), Alexa Fluor 647 donkey anti-rabbit (1:1000; Jackson ImmunoResearch, 711-605-152) and Cy3 donkey anti-rabbit (1:1,000; Jackson ImmunoResearch, 711-165-152). DAPI (Invitrogen, D1306; 0.5 $\mu\text{g ml}^{-1}$ in PBS) was used to stain nuclei.

FISH

smFISH (ACDBio, RNAscope) was used to detect the expression of *Nts*, *Gad2*, *Slc17a6* (*Vglut2*), *Fos* and *cre* in the IPAC and surrounding tissues of adult mice. For tissue preparation, mice were first anesthetized under isoflurane and then decapitated. Brain tissue was rapidly extracted, embedded in M-1 embedding matrix (Thermo Scientific, 1310) in cryomolds (Sakura Finetek, 4566) and fresh-frozen on dry ice. Brain tissue was cut on a cryostat (Leica, CM3050S) to obtain 16- μm sections, collected on slides (VWR Microslides Superfrost Plus, 48311-703) and stored at -80°C . Hybridization was performed using the RNAscope kit (ACDBio). The protocol was previously described⁴⁸. Probes against *Nts* (420441), *Gad2* (439371), *Slc17a6* (*Vglut2*; 319171), *Fos* (316921) and *cre* (312281) were applied at a 1:50 dilution to sections. Images were taken using an LSM710 or LSM780 confocal microscope (Carl Zeiss) and visualized and processed using ImageJ (1.53q) and Adobe Illustrator (CS6, version 16.0.0).

Fos experiments. Mice in the FR groups had their food removed at 1700 h the day before the testing day. Food was reintroduced to the mice 18 h after food restriction (between 1100 h and 1400 h). The foods used were regular chow (PicoLab rodent diet 20, 5053*) and a lard-based HFD (Bioserv HFD, S3282). Thirty minutes after food reintroduction, food consumption was recorded, and the mice were killed. The brain tissue was processed for RNAscope. Water (HydroGel, ClearH₂O) was available ad libitum until 3 h before the mice were killed. Mice and their brain tissues in different groups underwent the experimental procedure in parallel to minimize variability.

RNA extraction and quantitative PCR

Approximately 50 mg of fat tissue was collected using sterile instruments and frozen in 500 μl of Trizol (Thermo Fisher, 15596026) on dry ice and stored at -80°C until further processing. The tissue was then homogenized by adding a stainless steel bead (Qiagen, 69989) into each tube and shaking the tubes in a TissueLyser (TissueLyser II, Qiagen, 85300) two times for 2 min each at 30 Hz. After incubating the homogenate for 5 min on ice, 100 μl of chloroform (Sigma-Aldrich, C2432-1L) was added, and the tubes were shaken briefly. After incubating for 3 min on ice, the tubes were centrifuged at 12,000g at 4°C for 15 min. Subsequently, the clear top layer was transferred into a fresh tube, and one-tenth volume of 3 M sodium acetate (Bioworld, 41920024-4) and glycogen (Thermo Scientific, R0551) at a final concentration of 1 $\mu\text{g } \mu\text{l}^{-1}$ and 250 μl of isopropanol (Fisher Scientific, S25372) were added. The tubes were inverted to mix the contents, and after a 10-min incubation on ice, the tubes were centrifuged at 12,000g at 4°C for 10 min. The supernatant was discarded, and the RNA pellet was resuspended in 500 μl of 75% ethanol. After centrifuging at 7,500g at 4°C for 5 min, the supernatant was discarded, the RNA pellet was left to air dry for 5 min and was resuspended in 25 μl of RNase-free water. cDNA was synthesized from 500 ng of total RNA using TaqMan reverse transcription reagents (Thermo Fisher, N8080234). Quantitative PCR with reverse transcription was performed using a QuantStudio 6 Flex real-time PCR system using TaqMan Fast Advanced master mix (Thermo Fisher, 4444556) and TaqMan Primers. The 2^{- $\Delta\Delta\text{Ct}$} method was used to quantify

relative amounts of product, with a housekeeping gene (*Gapdh*) as an endogenous control. Primers used were *Gapdh* (Thermo Fisher, assay ID Mm99999915_g1, 4331182) and *Ucp1* (Thermo Fisher, assay ID Mm01244861_m1, 4331182).

Hematoxylin and eosin (H&E) staining

Tissues were fixed in 4% PFA for 24 h at 4°C , washed in PBS three times at room temperature and dehydrated in 70% ethanol. Subsequently, tissues were embedded in paraffin, serially cut using a microtome to produce 5- μm sections and stained with H&E. Images were acquired using a Zeiss Observer microscope equipped with $\times 10$, $\times 20$ and $\times 40$ lenses.

Oil red O staining

Livers were fixed in 4% PFA for 24 h at 4°C , washed in PBS three times at room temperature and cryopreserved in 30% sucrose in PBS. Tissues were embedded in OCT Tissue Tek (Sakura, 4583), and 10- μm sections were cut using a Leica cryostat. Oil red O staining was performed as previously described⁴⁹, including the counterstaining with hematoxylin (Abcam, ab220365). Images were acquired using a Zeiss Observer microscope equipped with $\times 10$, $\times 20$ and $\times 40$ lenses.

Statistical analysis

All statistics are described where used. Statistical analyses were conducted using GraphPad Prism 7 software (GraphPad). No statistical methods were used to predetermine sample sizes, but our sample sizes are similar to those reported in previous publications^{46,48,50}. Data distribution was assumed to be normal, but this was not formally tested. All *t*-tests were two tailed. Statistical hypothesis testing was conducted at a significance level of 0.05. All mice were randomly assigned to different groups, and data collection was randomized whenever possible. Data collection and analysis were not performed blind to the conditions of the experiments. Mice that, after histological inspection, had the location of the viral injection (reporter protein) or of the optic fiber(s) outside the area of interest were excluded.

Reporting summary

Further information on research design is available in the Nature Research Reporting Summary linked to this article.

Data availability

All data are contained in the main text, Extended Data or Supplementary Information. Source data are provided with this paper.

Code availability

Custom code is available on GitHub at <https://github.com/Alefurlan/IPACpaper>.

References

- Stephenson-Jones, M. et al. A basal ganglia circuit for evaluating action outcomes. *Nature* **539**, 289–293 (2016).
- Zhang, X. & Li, B. Population coding of valence in the basolateral amygdala. *Nat. Commun.* **9**, 5195 (2018).
- Gamba, O. F. M. BORIS: a free, versatile open-source event-logging software for video/audio coding and live observations. *Methods Ecol. Evol.* **7**, 1325–1330 (2016).
- Xiao, X. et al. A genetically defined compartmentalized striatal direct pathway for negative reinforcement. *Cell* **183**, 211–227 (2020).
- Mehlem, A., Hagberg, C. E., Muhl, L., Eriksson, U. & Falkevall, A. Imaging of neutral lipids by oil red O for analyzing the metabolic status in health and disease. *Nat. Protoc.* **8**, 1149–1154 (2013).
- Stephenson-Jones, M. et al. Opposing contributions of GABAergic and glutamatergic ventral pallidal neurons to motivational behaviors. *Neuron* **105**, 921–933 (2020).

Acknowledgements

We thank T. Russo for technical assistance and members of the Li laboratory for helpful discussions. This work was supported by grants from EMBO (ALTF 458–2017, A.F.), the Swedish Research Council (2017-00333, A.F.), the Charles H. Revson Senior Fellowship in Biomedical Science (19–23, A.F.), the National Institutes of Health (R01MH101214, R01MH108924, R01DA050374 and R01NS104944, B.L.), the Cold Spring Harbor Laboratory and Northwell Health Affiliation (B.L.), the Feil Family Neuroscience Endowment (B.L.) and the German Academic Scholarship Foundation (E.C.G.).

Author contributions

A.F. and B.L. conceived and designed the study. A.F. conducted the experiments and analyzed data. A.C. assisted with the photometry experiments with food odors and the data analysis. S. Boyle set up behavioral rigs and generated MATLAB code for controlling behavioral devices and analyzing photometry data. R.S. assisted with the smFISH experiments. R.R. and J.H. assisted with operating the metabolic cages. E.C.G. assisted with the GTT and ITT experiments. R.S. and E.C.G. collected tissue samples and performed quantitative PCR experiments. J.G. assisted with the EPM and OF experiments. S. Beyaz provided critical reagents. T.J. supervised the experiments by E.C.G. and assisted with interpreting metabolic data. S.D.S. supervised the

experiments by A.C. and assisted with analyzing and interpreting the data. A.F. and B.L. wrote the paper with input from all authors.

Competing interests

The authors declare no competing interests.

Additional information

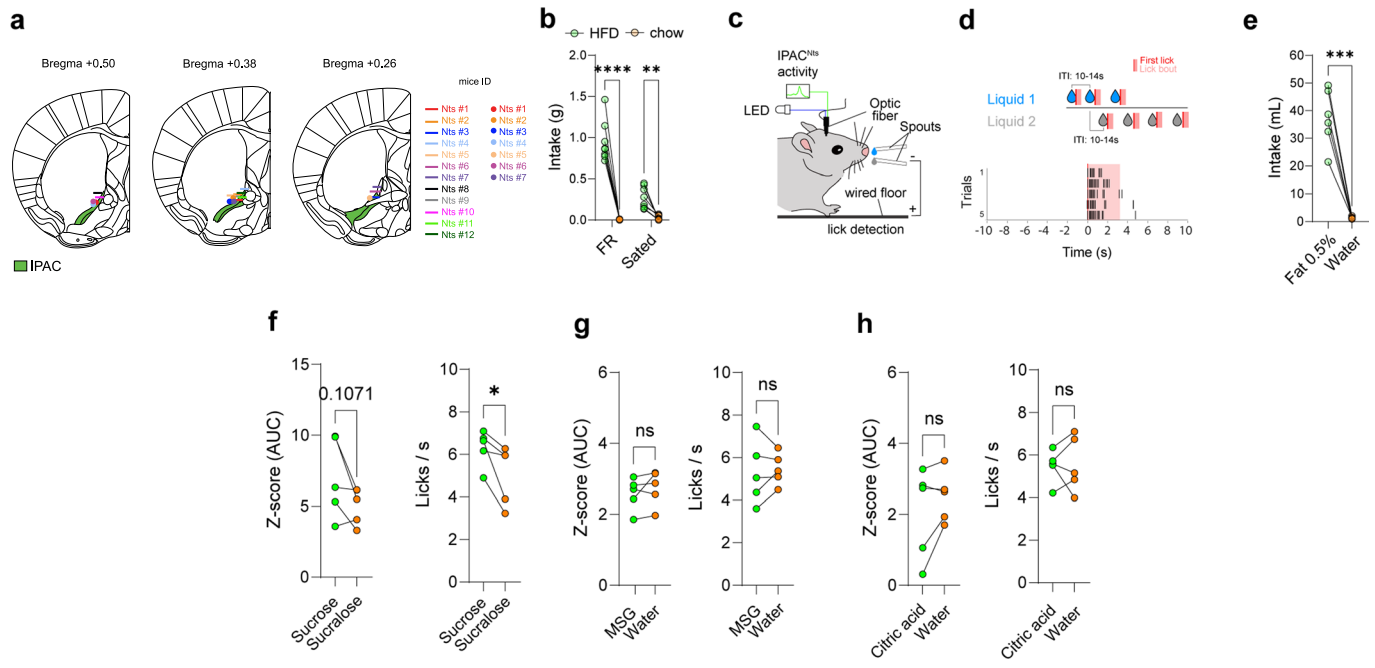
Extended data is available for this paper at <https://doi.org/10.1038/s41593-022-01178-3>.

Supplementary information The online version contains supplementary material available at <https://doi.org/10.1038/s41593-022-01178-3>.

Correspondence and requests for materials should be addressed to Alessandro Furlan or Bo Li.

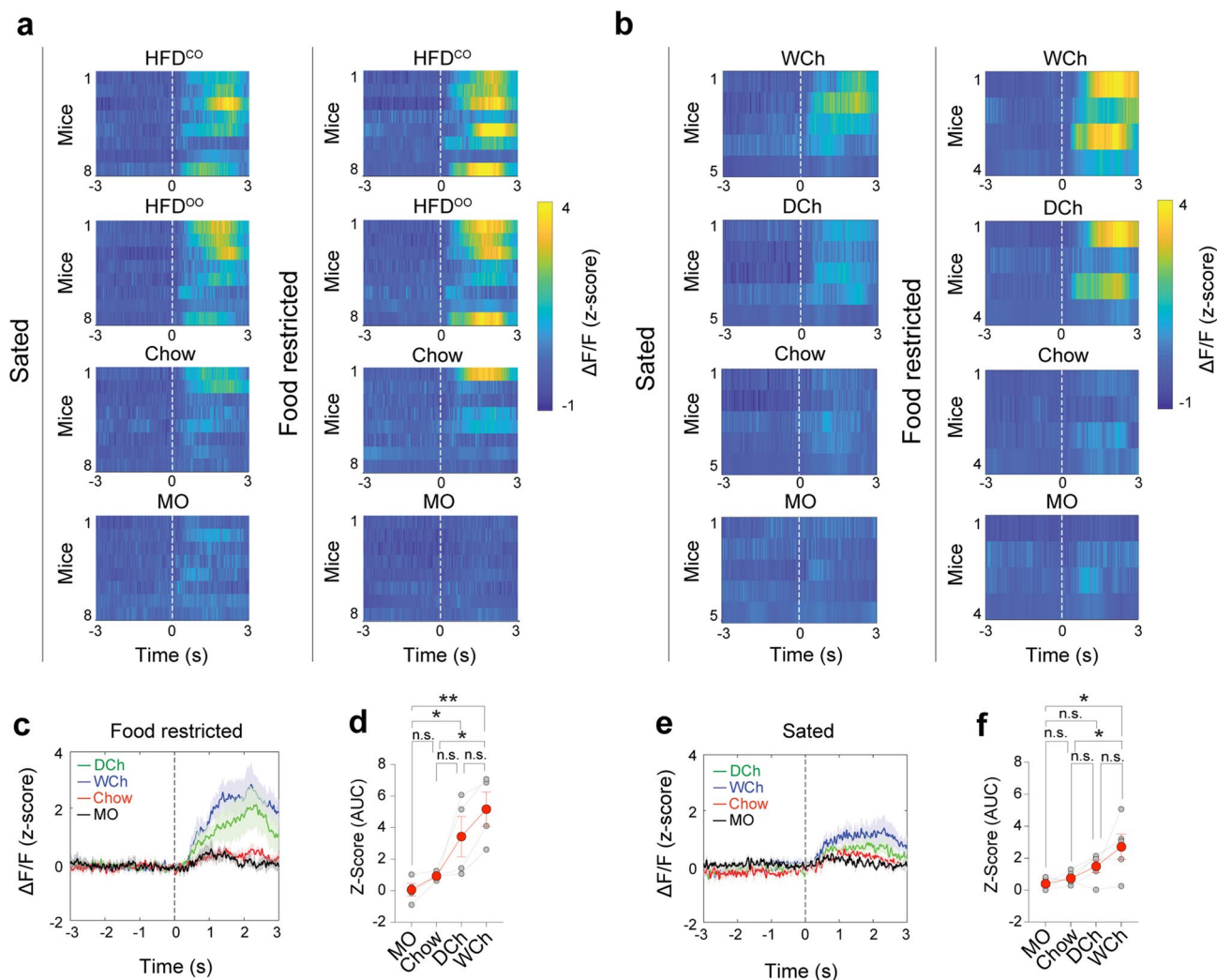
Peer review information *Nature Neuroscience* thanks Roger Adan, Alexander Nectow, and the other, anonymous, reviewer(s) for their contribution to the peer review of this work.

Reprints and permissions information is available at www.nature.com/reprints.



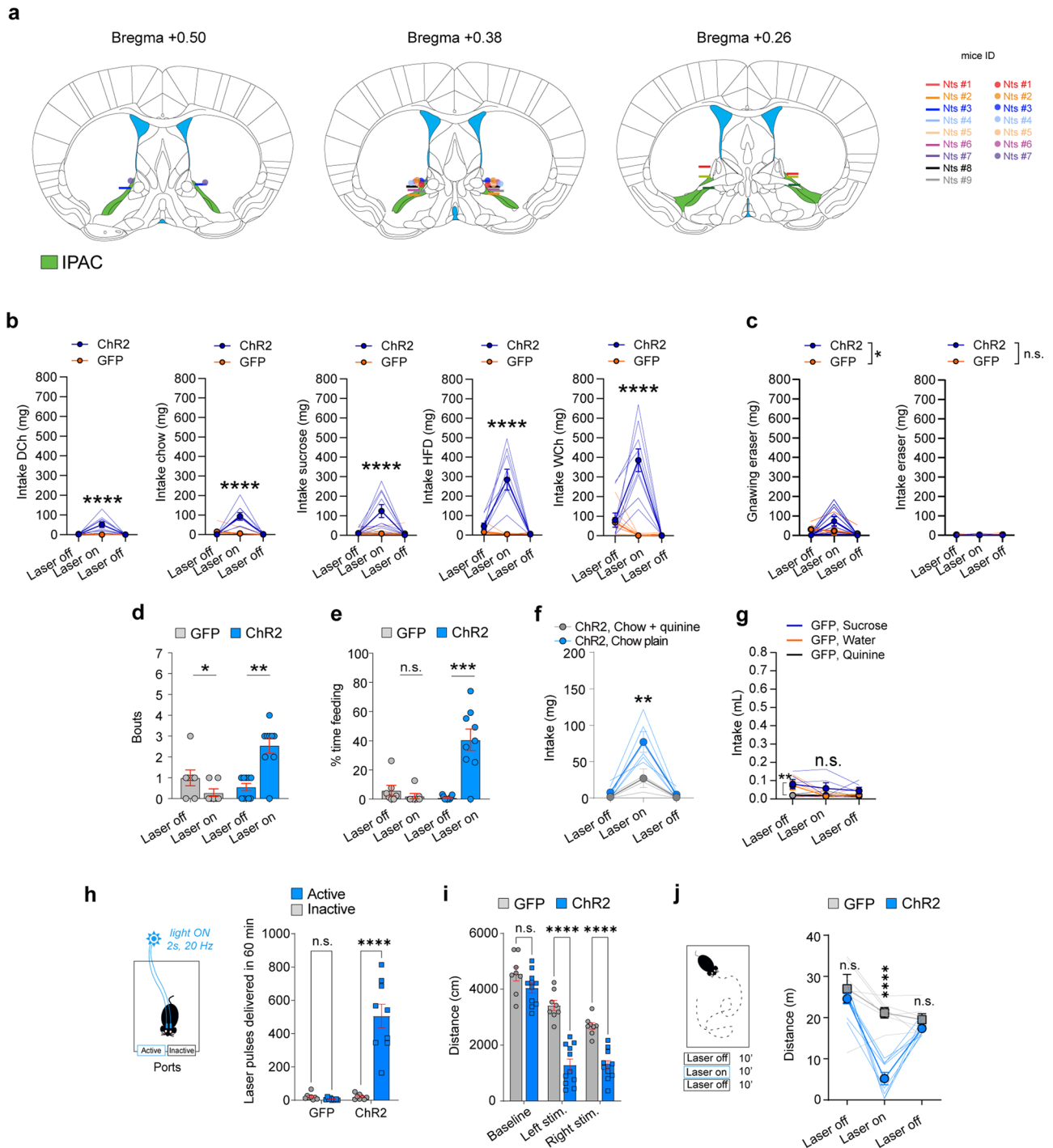
Extended Data Fig. 1 | IPAC^{Nts} neurons encode the hedonic value of a stimulus. (a) Schematics showing the locations of optic fiber placement in the mice used in Figs. 2 and 3. (b) Feeding behavior of mice when presented with HFD (green) or chow (orange), for 20 minutes, in food restricted (FR, left) or sated condition (right). N = 8. Group effect: $F_{(1,7)}=95.19$, $p < 0.0001$, $**p < 0.01$, $****p < 0.0001$; Two-way RM ANOVA, Sidak's test. (c, d) Schematics of the experimental setup (c) and task structure (d) used in Fig. 2. Bottom panel: representative raster plot showing licking behavior following liquid delivery. (e) Drinking behavior of wild-type mice when presented with Intralipid 0.5% (Fat 0.5%, green) or water (orange), in a 2-bottle preference test, for 72-h, in sated condition. N = 6 mice. $***P = 0.0003$,

paired t-test. (f-h) Food-restricted (FR) mice (f) and water-restricted (WR) mice (g, h) were presented with equal volumes of liquids in the same session. Left: Area under the curve (AUC) of GCAMP6f signals. Right: licking behavior (behavior) of mice. AUC and licking behavior were measured in a 3-s window following the first lick. Paired t-tests, $n = 5$ mice/group in all panels. (f) Sucrose (green) or sucralose (orange); AUC: $p = 0.1071$ (n.s.); Behavior: $*p = 0.0462$. (g) Monosodium glutamate (MSG, green) or water (orange); AUC: $p = 0.3008$ (n.s.); Behavior: $p = 0.7061$ (n.s.). (h) Citric acid (green) or water (orange); AUC: $p = 0.1997$ (n.s.); Behavior: $p = 0.8677$ (n.s.).



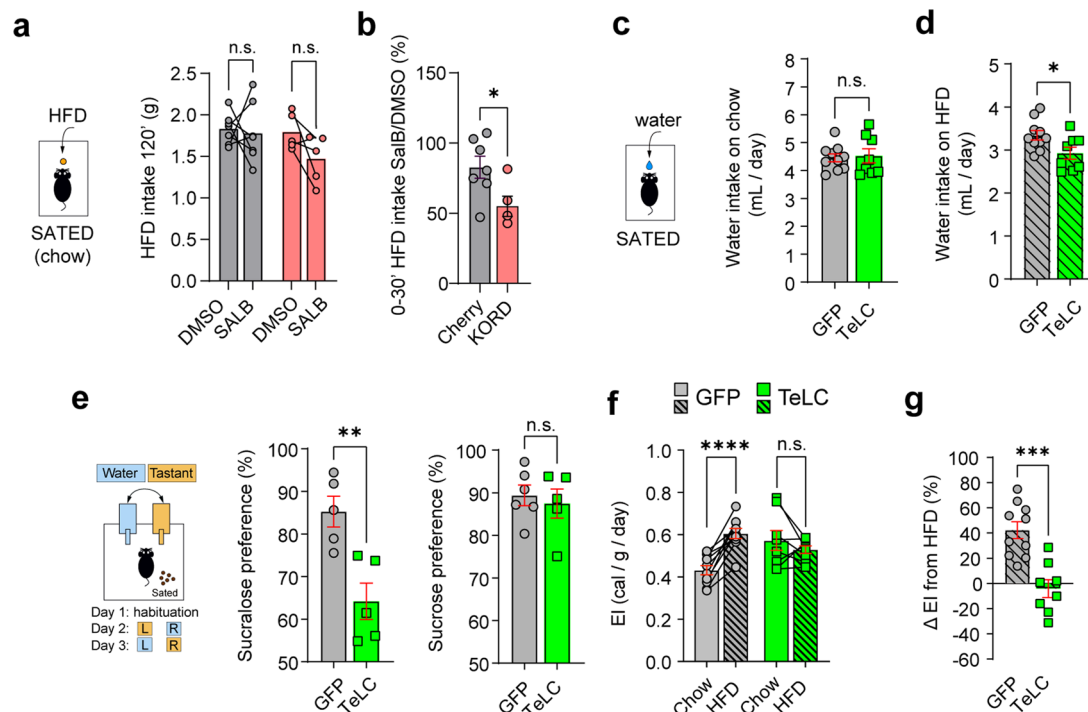
Extended Data Fig. 2 | Response of IPAC^{Nts} neurons to odors from several diets. (a, b) Heatmaps of the response of IPAC^{Nts} neurons in individual mice to odors derived from different food sources, under sated or food-restricted condition, as indicated. Dashed lines indicate the onset of odor presentation. (c) Average GCaMP6f signals from IPAC^{Nts} neurons in food-restricted mice aligned to the presentation of different odors (dashed line). (d) Area under the curve (AUC) of the responses in individual mice in (c) in a 3-s window following

odor presentation. $N = 4$ mice. $F_{(3,9)} = 10.36$, $p = 0.0028$; * $p < 0.05$, ** $p < 0.01$, n.s., $p > 0.05$; one-way RM ANOVA, Holm-Sidak's test. (e) Average GCaMP6f signals from IPAC^{Nts} neurons in sated mice aligned to odor presentation (dashed line). (f) Area under the curve (AUC) of the responses in individual mice in (e) in a 3-s window following odor presentation. $N = 5$ mice. $F_{(3,12)} = 5.169$, $p = 0.0160$; * $p < 0.05$, $p > 0.05$ (n.s.); one-way RM ANOVA, Holm-Sidak's test.



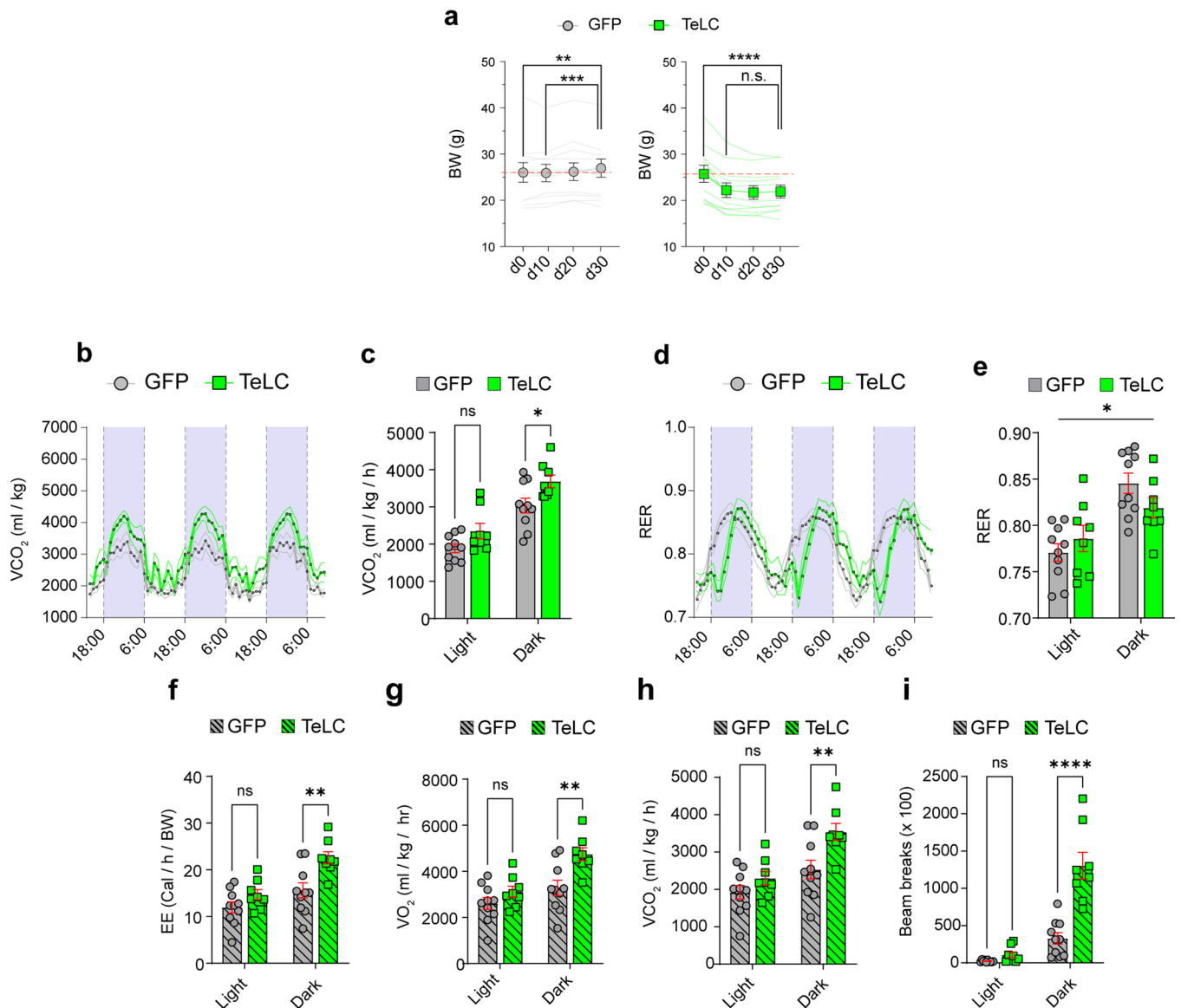
Extended Data Fig. 3 | Characterization of behavioral effects following activation of IPAC^{Nts} neurons. (a) Optic fiber placement for mice in Fig. 4. (b) Effect of photostimulation of IPAC^{Nts} neurons in mice fed dark chocolate (DCh), chow, sucrose, HFD, white chocolate (WCh). ChR2 (n = 9) or GFP (n = 6) for DCh, ChR2 (n = 9) or GFP (n = 8) for chow, sucrose, HFD, WCh. Two-way RM ANOVA, Sidak's test. DCh, group effect: $F_{(1,13)}=7.374$, $p = 0.0177$; chow, group effect: $F_{(1,15)}=8.999$, $p = 0.0090$; sucrose, group effect: $F_{(1,15)}=7.829$, $p = 0.0135$; HFD, group effect: $F_{(1,15)}=21.22$, $p = 0.0003$; WCh, group effect: $F_{(1,15)}=22.56$, $p = 0.0003$. (c) Effect of photostimulation of IPAC^{Nts} neurons in mice presented with an inedible pencil eraser. ChR2 (n = 9) or GFP (n = 6). two-way RM ANOVA, Sidak's test. Gnawing, interaction effect: $F_{(2,26)}=4.939$, $p = 0.0152$; intake: $F_{(2,26)}=1.066$, $p = 3591$ (n.s.). **** $p < 0.0001$; $p > 0.05$ (n.s.). (d, e) Photostimulation of IPAC^{Nts} neurons increased the number (d) and the duration (e) of feeding bouts in ChR2 (n = 9) but not GFP mice (n = 7). (d) GFP: * $p = 0.0465$, ChR2: ** $p = 0.0028$; (e) GFP:

$p = 0.0982$ (n.s.), ChR2: **** $p = 0.0007$, paired t-test. (f) Effect of photostimulation of IPAC^{Nts} neurons in ChR2 mice fed quinine-flavored or plain chow pellets (n = 5). Interaction effect: $F_{(2,8)}=9.476$, $p = 0.0078$, ** $p < 0.01$, two-way RM ANOVA, Sidak's comparisons test. (g) Effect of photostimulation of IPAC^{Nts} neurons on liquid consumption (control for Fig. 4e). GFP mice (n = 5), interaction effect: $F_{(4,16)}=1.119$, $p = 0.3820$ (n.s.). Two-way RM ANOVA. (h) Self-stimulation paradigm (left) and quantification of the poking responses of ChR2 (n = 9) and GFP mice (n = 8). Group effect: $F_{(1,15)}=37.63$, $p < 0.0001$; **** $p < 0.0001$; $p > 0.05$ (n.s.), two-way RM ANOVA, Sidak's test. (i) Distance traveled in the RTTPP/A task. ChR2 (n = 11) and GFP (n = 8) mice. Group effect: $F_{(1,17)}=34.11$, $p < 0.0001$; **** $p < 0.0001$; $p > 0.05$ (n.s.), two-way RM ANOVA, Sidak's test. (j) Distance traveled in the open field test. ChR2 (n = 8) and GFP (n = 6) mice. Group effect: $F_{(1,12)}=17.30$, $p = 0.0013$; **** $p < 0.0001$; $p > 0.05$ (n.s.) two-way RM ANOVA, Sidak's test.



Extended Data Fig. 4 | Inactivation of IPAC^{Nts} neurons impairs hedonic perception. **(a)** HFD intake over a 2-h period in sated *Nts^{Cre}* mice expressing mCherry (gray, control) or KORD (red) injected with DMSO or SaLB. mCherry mice, $n = 7$; KORD mice, $n = 5$. paired t-test. Cherry DMSO-SaLB: $p = 0.7748$, (n.s.); KORD DMSO-SaLB: $p = 0.1066$ (n.s.). Paired t-test. **(b)** Percentage change of HFD intake in food-restricted mice expressing mCherry (gray, control) or KORD (red) when injected with SaLB, normalized to their intake when injected with DMSO, within 30 minutes from food presentation. mCherry mice, $n = 7$; KORD mice, $n = 5$. * $p = 0.0326$. Unpaired t-test. **(c)** Daily water intake of the GFP mice ($n = 10$) and TeLC mice ($n = 8$) fed chow. $p = 0.8023$ (n.s.), unpaired t-test.

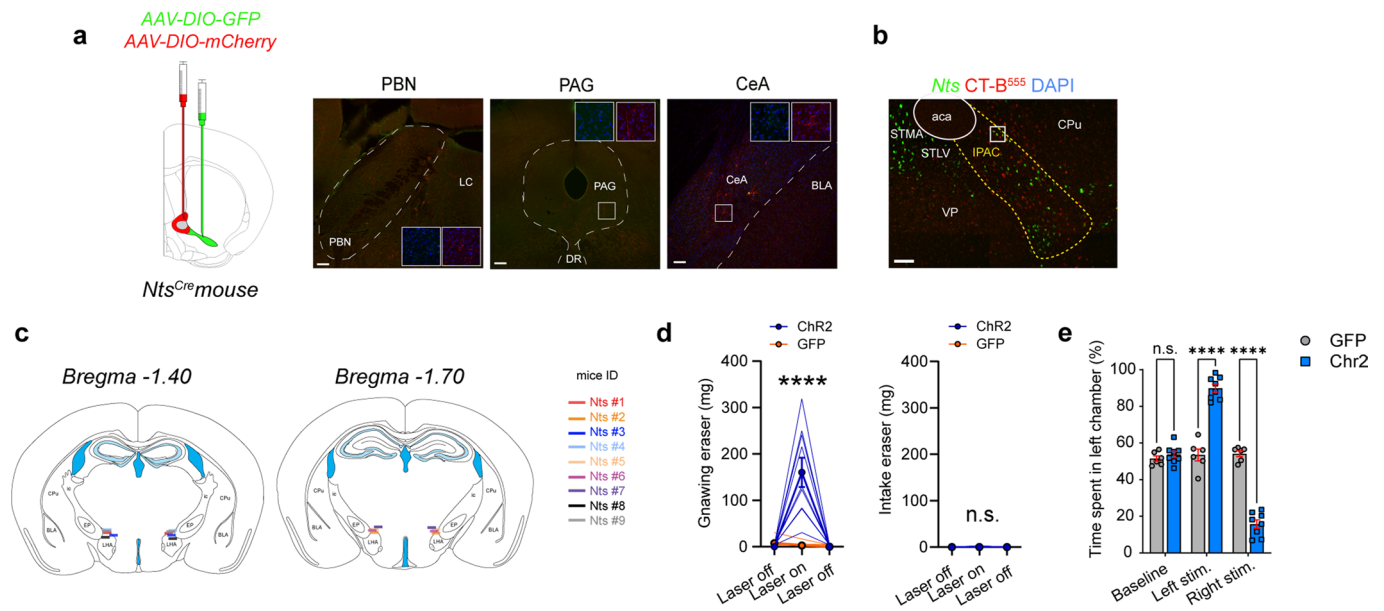
(d) Daily water intake of the GFP mice ($n = 10$) and TeLC mice ($n = 8$) fed HFD. * $p = 0.0305$, unpaired t-test. **(e)** Schematic of the 2-bottle preference test (left) for sucralose (center) and sucrose (right). Sucralose: GFP mice ($n = 5$), TeLC mice ($n = 5$): ** $p = 0.0055$, unpaired t-test. Sucrose: GFP mice ($n = 6$); TeLC mice ($n = 5$); $p = 0.6488$ (n.s.), unpaired t-test. Legend: L, left bottle, R, right bottle. **(f)** Comparison of energy intake from chow and HFD diets (derived from Fig. 5i and j). GFP ($n = 10$): **** $p < 0.0001$; TeLC mice ($n = 8$): $p = 0.3562$ (n.s.); paired t-test. **(g)** Change in energy intake after the switch from chow to HFD. *** $P = 0.0002$, unpaired t-test.



Extended Data Fig. 5 | Inactivation of IPAC^{Nts} neurons has positive metabolic effects.

(a) Changes in body weight (BW) following injection (d0). GFP mice (n = 11): $F(3, 30) = 6.588$, $p = 0.0015$; ** $p < 0.01$; *** $p < 0.001$; TeLC mice (n = 10): $F(3, 27) = 28.11$, $p < 0.0001$; **** $p < 0.0001$, $p > 0.05$ (n.s.); one-way RM ANOVA, Sidak's test. **(b)** Volume of carbon dioxide produced (VCO₂) by GFP (n = 10) and TeLC mice (n = 8). Group effect: $F_{(1,16)} = 5.745$, $p = 0.0291$, two-way RM ANOVA, Sidak's test. **(c)** Average carbon dioxide production (VCO₂) of the mice in (b). GFP (n = 10); TeLC (n = 8). Group effect: $F_{(1,16)} = 5.603$, $p = 0.0309$; * $p < 0.05$, $p > 0.05$ (n.s.); two-way RM ANOVA, Sidak's test. **(d)** Respiratory exchange ratio (RER) of GFP (n = 10) and TeLC mice (n = 8). Interaction effect: $F_{(70,1120)} = 5.042$, $p < 0.0001$, two-way RM ANOVA. **(e)** Average RER of GFP (n = 10) and TeLC mice (n = 8) fed chow.

Interaction effect: $F_{(1,16)} = 7.546$, * $p = 0.0143$; two-way RM ANOVA, Sidak's test. **(f)** Average energy expenditure of GFP (n = 10) and TeLC mice (n = 8) fed HFD. Group effect: $F_{(1,16)} = 6.526$, $p = 0.0212$; * $p < 0.05$, n.s., $p > 0.05$; two-way RM ANOVA, Sidak's test. **(g)** Average oxygen consumption (VO₂) of GFP (n = 10) and TeLC mice (n = 8) fed HFD. Group effect: $F_{(1,16)} = 6.066$, * $p = 0.0255$, $p > 0.05$ (n.s.); two-way RM ANOVA, Sidak's test. **(h)** Average carbon dioxide production (VCO₂) of GFP (n = 10) and TeLC mice (n = 8) fed HFD. Group effect: $F_{(1,16)} = 5.276$, * $p = 0.0355$, $p > 0.05$ (n.s.); two-way RM ANOVA, Sidak's test. **(i)** Average locomotor activity of GFP (n = 10) and TeLC mice (n = 8) fed HFD. Group effect: $F_{(1,16)} = 25.21$, $p < 0.0001$; **** $p < 0.0001$, $p > 0.05$ (n.s.), two-way RM ANOVA, Sidak's test.



Extended Data Fig. 6 | Network of IPAC^{Nts} neurons. (a) Representative images of brain areas innervated by IPAC^{Nts} (green) and mBST^{Nts} (red) neurons. Scale bar: 100 μ m. STLV: ventral lateral division of the BNST; STMA: anterior medial division; VP: ventral pallidum; CPU: caudate putamen; IPAC: interstitial nucleus of the posterior limb of the anterior commissure (aca); LC: locus coeruleus; PBN: parabrachial nu.; CeA: central amygdala; BLA: basolateral amygdala; PAG: periaqueductal gray; DR: dorsal raphe. (b) Representative image of smFISH for *Nts* on retrograde labelled CT-B⁺ neurons in the IPAC. The square in the image show the high-magnification area showed in Fig. 7h (right). Scale bar: 100 μ m.

(c) Schematics showing the locations of optic fiber placement in the mice used in Fig. 7. (d) Effect of light delivery into the IPAC of the ChR2 (n = 9) or GFP (n = 5) mice on gnawing (left) and consumption (right) of inedible items (that is, pencil eraser). Gnawing (group effect): $F_{(1,12)}=11.51$, $p = 0.0053$, two-way RM ANOVA, Sidak's test. **** $p < 0.0001$. Intake: (group effect): $F_{(1,12)}=0.5327$, $p = 4783$, two-way RM ANOVA. (e) Preference of ChR2 (n = 8) and GFP mice (n = 6) for the left chamber side. Interaction effect: $F_{(2,24)}=125.1$; $p < 0.0001$; **** $p < 0.0001$; $p > 0.05$ (n.s.). Two-way RM ANOVA, Sidak's test.

Reporting Summary

Nature Portfolio wishes to improve the reproducibility of the work that we publish. This form provides structure for consistency and transparency in reporting. For further information on Nature Portfolio policies, see our [Editorial Policies](#) and the [Editorial Policy Checklist](#).

Statistics

For all statistical analyses, confirm that the following items are present in the figure legend, table legend, main text, or Methods section.

n/a Confirmed

- The exact sample size (n) for each experimental group/condition, given as a discrete number and unit of measurement
- A statement on whether measurements were taken from distinct samples or whether the same sample was measured repeatedly
- The statistical test(s) used AND whether they are one- or two-sided
Only common tests should be described solely by name; describe more complex techniques in the Methods section.
- A description of all covariates tested
- A description of any assumptions or corrections, such as tests of normality and adjustment for multiple comparisons
- A full description of the statistical parameters including central tendency (e.g. means) or other basic estimates (e.g. regression coefficient) AND variation (e.g. standard deviation) or associated estimates of uncertainty (e.g. confidence intervals)
- For null hypothesis testing, the test statistic (e.g. F , t , r) with confidence intervals, effect sizes, degrees of freedom and P value noted
Give P values as exact values whenever suitable.
- For Bayesian analysis, information on the choice of priors and Markov chain Monte Carlo settings
- For hierarchical and complex designs, identification of the appropriate level for tests and full reporting of outcomes
- Estimates of effect sizes (e.g. Cohen's d , Pearson's r), indicating how they were calculated

Our web collection on [statistics for biologists](#) contains articles on many of the points above.

Software and code

Policy information about [availability of computer code](#)

Data collection

Data regarding food and liquid consumption was obtained weighing food pellets and liquids before and after each testing session.

c-Fos experiments: mice in the food-restriction (FR) groups had the food was removed at 5 p.m. the day before the testing day. Food was reintroduced to the mice 18-20 h after food-restriction (between 11 a.m. and 2 p.m.). The foods used were regular chow (PicoLab Rodent Diet 20, Cat. No. #5053*) and lard-based HFD (Bioserv HFD, Cat. No. # S3282). At 30 minutes after the food reintroduction, food consumption was recorded, and the mice were sacrificed. The brain tissue was processed for RNAscope. Water (Hydrogel, ClearH2O) was available ad libitum until 3 h before the mice were sacrificed. Mice and their brain tissues in different groups underwent the experimental procedure in parallel to minimize variability.

Single molecule fluorescent in situ hybridization was performed using RNAscope (ACDBio). Immunohistochemistry was performed following standard procedures (Stephenson-Jones, M. et al. Nature, 2016).

Fiber photometry data relative to taste and feeding experiments was collected by a commercial fiber photometry system (Neurophotometrics Ltd) with Bonsai software (Bonsai, version 2.3.1). Signals from each fiber were corrected for photobleaching by fitting the decay with a double exponential to calculate dF/F , then normalized by calculating Z score. Photometry data relative to odor experiment was acquired with a custom-made fiber photometry system to measure GCaMP6f signals in vivo and an olfactometer. Green and red emitted fluorescence signals were filtered and split to separate photodetectors and digitally sampled at 6100 Hz via a data acquisition board (National Instruments, Model # NI USB-6211). Peaks were extracted by custom Matlab software with an effective sampling rate of 211 Hz. The red signals reflect autofluorescence and were used to monitor and correct for potential movement artifacts.

Optogenetics experiments: on the testing day, following habituation, a food pellet or a liquid (in a metal cup) was placed on the floor of the box. Feeding behavior was assessed for 5 minutes with laser off (baseline measure), then 5 minutes with light on (20Hz, 7-10 mW measured at the tip of the fiber), and then another 5 minutes with laser off. The foods used were: grain-based pellets (similar to the regular chow; 45 mg/pellet, Bioserv, F0165, 3.43 cal/g), sucrose (45 mg/pellet, Bioserv, F0021, 3.83 cal/g), high fat diet (HFD) (soft pellet, Bioserv, S3282, 5.49

cal/g), white chocolate (Lindt, 5.5 cal/g), dark chocolate (Ghirardelli, 5.5 cal/g), HFD-CO (Envigo custom diet, 4.5 cal/g), HFD-OO (Envigo custom diet, 4.5 cal/g). Plain and quinine-flavored grain-based pellets were prepared by immersing the pellets in either water or a 10 mM quinine solution for 10 minutes. Pellets were dried overnight and used for testing the following day. Diets were presented either on consecutive days or within the same session (Methods) to sated mice. Liquids used were: 30% sucrose in water (w/v), 10% sucrose in water (w/v), 0.1% sucralose in water (w/v), 5% fat emulsion (intralipid), NaCl 75mM in water (w/v), 10 mM Citric Acid in water, Quinine 1 mM in water and water.

Chemogenetic experiments: experimental KORD and control mCherry mice were given a subcutaneous (s.c.) injection of SalB (10 mg / Kg in DMSO) or control vehicle (DMSO, volume equivalent). After the injection, mice were placed back in their home cage for 20 minutes before starting testing (e.g. food was introduced to the cage).

Food preference tests: mice were familiarized with the diets, introduced in the home cage on consecutive days, with chow and water available ad libitum. Mice were singly housed. On the test days, both diets were presented simultaneously in the home cage and intake was measured at 3 h after the delivery.

Liquid preference tests: sated mice were singly housed with food and water available ad libitum for a week before the start of the experiment. Water was dispensed through a bottle in the cage. After this, a second bottle containing either the sucralose or sucrose solution was added to the cage. Mice were allowed to first habituate to the newly added solution for 24-h, after which their consumption of the solution and water over a 48-h period was measured. The testing of sucralose and sucrose was separated by a 48-h period, during which the mice had access only to water. The positions of the bottles were switched every 24-h to minimize a potential positional effect.

Conditioned flavor preference: Single housed mice sated on chow were familiarized to the coco and olive- based lard diets in 2 consecutive days. The baseline flavor preference was assessed by presenting mice with the two diets at the same time. Food preference was determined based on their 3h intake, over the second of 2 consecutive test days. Conditioning was carried out for 4 days, with 2 sessions per day. Prior to each session, mice were tethered to the optic-fiber patch cable and habituated to the behavioral chamber for 10 minutes. Conditioning consisted in pairing intracranial light pulses (473 nm, 8-10mW, 30Hz) with the less preferred diet (session 1). 4h later, the same mice were presented with the more preferred diet without photostimulation (session 2). The order of the sessions was inverted every day. Photo stimulation was delivered right after the mouse would spontaneously initiate food intake and lasted for as long as the pellet was consumed (each was 0.5 g). The investigator manually delivered the light pulses. Conditioned flavor preference was tested for 2 consecutive days after conditioning (day 5 and day 6). The preference of these 2 sessions was averaged.

The RTPP, open field and elevated plus maze behaviors of the mice were videotaped with a CCD camera (C930, Logitech) interfaced with Ethovision software (XT 5.1, Noldus Information Technologies, Wageningen, The Netherlands).

Metabolic profiles were acquired using Columbus Instruments Comprehensive Lab Animal Monitoring System (CLAMS). Mice used in the control and inhibition groups (i.e. TeLC) were age-matched. Blood glucose levels in GTT and ITT tests were measured in duplicates at 0, 15, 30, 45, 60, 90, and 120 minutes after injection using OneTouch Ultra 2 Glucometer (OneTouch). Tissue used for qPCR experiments and histology was collected from the same mice tested in metabolic cages, GTT and ITT, at endpoint.

H&E Staining: tissues were fixed in 4% PFA for 24 h at 4°C, washed in PBS three times at room temperature and dehydrated in 70% ethanol. Subsequently, tissues were embedded in paraffin, cut using a microtome serially and stained with Hematoxylin and Eosin (H&E). Pictures were taken using a Zeiss Observer microscope equipped with 10x, 20x and 40x lenses.

Oil Red O staining: livers were fixed in 4% PFA for 24 h at 4°C, washed in PBS three times at room temperature and cryopreserved in 30% sucrose. Tissues were embedded in OCT tissue tek (Sakura, Cat. No. #4583) and were cut using a Leica Cryostat. Oil Red O staining was performed as previously described 58 including the counterstaining with Hematoxylin. Pictures were taken using a Zeiss Observer microscope equipped with 10x, 20x and 40x lenses.

Data analysis

Images (including those for FISH, H&E, Oil Red O, histology) were analyzed using ImageJ (V1.53q). For behavioral scoring (e.g. bouts lengths), we used the Behavioral Observation Research Interactive Software (BORIS v 7.12.2). All fiber photometry and decoding data were analyzed with custom-written scripts in Matlab (Mathworks, R2017a, available on Github). Data regarding food and liquid consumption was obtained weighing food pellets and liquids before and after each testing session. Statistical analyses were performed and plotted with Matlab or Prism7.

(GraphPad). Metabolic data was visualized and analyzed using Excel (2019) and the CLAMS Examination Tool (Clax software v2.2.0).

For manuscripts utilizing custom algorithms or software that are central to the research but not yet described in published literature, software must be made available to editors and reviewers. We strongly encourage code deposition in a community repository (e.g. GitHub). See the Nature Portfolio [guidelines for submitting code & software](#) for further information.

Data

Policy information about [availability of data](#)

All manuscripts must include a [data availability statement](#). This statement should provide the following information, where applicable:

- Accession codes, unique identifiers, or web links for publicly available datasets
- A description of any restrictions on data availability
- For clinical datasets or third party data, please ensure that the statement adheres to our [policy](#)

All data is contained in the main text or supplementary data. The custom code that support the findings from this study are available from the corresponding authors upon request.

Field-specific reporting

Please select the one below that is the best fit for your research. If you are not sure, read the appropriate sections before making your selection.

- Life sciences Behavioural & social sciences Ecological, evolutionary & environmental sciences

Life sciences study design

All studies must disclose on these points even when the disclosure is negative.

Sample size	No statistical methods were used to pre-determine sample sizes but our sample sizes are similar to those reported in previous publications (Xiao, X., et al., 2020; Stephenson-Jones, M., et al., 2020; Zhang, X. & Li, 2018).
Data exclusions	Mice that, after histological inspection, had the location of the viral injection (reporter protein) or of the optic fiber(s) outside the area of interest, were excluded.
Replication	To ensure that results are reproducible, we included in the manuscript methods all details relative to softwares, reagents, and protocols. We plotted individual data points and provided source data. Information about the statistical test used is reported in the figure legends.
Randomization	All mice were randomly assigned to different groups. For food experiments, the order of presentation of the diets was randomized.
Blinding	Data collection and analysis were not performed blind to the conditions of the experiments. However, equal parameter and process were applied for all groups. Further, most behavioral experiments were controlled by automated computer systems (e.g. CLAMS) and the relative data were collected and analyzed in an unbiased way.

Reporting for specific materials, systems and methods

We require information from authors about some types of materials, experimental systems and methods used in many studies. Here, indicate whether each material, system or method listed is relevant to your study. If you are not sure if a list item applies to your research, read the appropriate section before selecting a response.

Materials & experimental systems

n/a	Involved in the study
<input type="checkbox"/>	<input checked="" type="checkbox"/> Antibodies
<input checked="" type="checkbox"/>	<input type="checkbox"/> Eukaryotic cell lines
<input checked="" type="checkbox"/>	<input type="checkbox"/> Palaeontology and archaeology
<input type="checkbox"/>	<input checked="" type="checkbox"/> Animals and other organisms
<input checked="" type="checkbox"/>	<input type="checkbox"/> Human research participants
<input checked="" type="checkbox"/>	<input type="checkbox"/> Clinical data
<input checked="" type="checkbox"/>	<input type="checkbox"/> Dual use research of concern

Methods

n/a	Involved in the study
<input checked="" type="checkbox"/>	<input type="checkbox"/> ChIP-seq
<input checked="" type="checkbox"/>	<input type="checkbox"/> Flow cytometry
<input checked="" type="checkbox"/>	<input type="checkbox"/> MRI-based neuroimaging

Antibodies

Antibodies used	The primary antibodies used were chicken anti-GFP (Aves Labs, GFP1020, dilution 1:1000), rabbit anti-RFP (1:1,000; Rockland, 600-401-379, 35868), rabbit anti-HA-tag (1:1,000; Cell Signaling, 37245), rabbit anti-mCherry (1:1,000; Abcam, ab167453, GR3213077-3); goat-anti AGRP (1:200, R&D, AF634). The secondary antibodies used were: Alexa Fluor 488 donkey anti-chicken (1:1000; Cat. number 703-545-155, Jackson ImmunoResearch); Alexa Fluor 647 donkey anti-chicken (1:1000; Cat. Number 703-606-155, Jackson ImmunoResearch); Alexa Fluor 647 donkey anti-goat IgG (1:1000; Cat. number 703-605-003, Jackson ImmunoResearch); Cy3 donkey rabbit (1:1000; Cat. Number 711-165-152, Jackson ImmunoResearch). DAPI (4',6-diamidino-2-phenylindole, Invitrogen, catalogue number D1306) (0.5 µg/ml in PBS) was used to stain nuclei.
Validation	The primary and secondary antibody used in this study were previously validated in the lab (e.g., Stephenson-Jones et al, 2016, Nature; Zhang and Li, 2018, Nature Communications; Stephenson-Jones et al, 2020, Neuron), and/or by the manufacturers.

Animals and other organisms

Policy information about [studies involving animals](#); [ARRIVE guidelines](#) recommended for reporting animal research

Laboratory animals	Male and female with age of of at least 2 months of age were used in all the experiments. The NtsCre mouse line (Stock No: 017525), Ai14 (Stock No: 007908) and wild-type mice (Stock No:000664) were purchased from Jackson Laboratories and bred onto a C57BL/6J background.
Wild animals	The study did not involve wild animals.
Field-collected samples	The study did not involve samples collected from the field.
Ethics oversight	Institutional Animal Care and Use Committee of Cold Spring Harbor Laboratory.

Note that full information on the approval of the study protocol must also be provided in the manuscript.